International Journal of Earth Sciences (2024) 113:23–47
https://doi.org/10.1007/s00531-023-02356-9

ORIGINAL PAPER

Provenance of far-traveled nappes in the eastern Mediterranean (Uppermost Unit, Crete): constraints from U–Pb zircon ages of detrital and igneous zircons

G. Zulauf[1] · W. Dörr[1] · R. Albert[2] · S. O. Martha[3] · P. Xypolias[4]

Received: 14 July 2023 / Accepted: 3 October 2023 / Published online: 4 November 2023

Abstract
New U–Pb ages of detrital and igneous zircons of the Uppermost Unit of Crete shed light on its provenance and on Eohellenic to Eoalpine imprints in the eastern Mediterranean. The detrital zircons of all nappes show Variscan ages and are characterized by a Minoan-type age spectrum, which is typical for the NE margin of Gondwana. Parts of the metasedimentary rocks are unexpectedly young. Their detrital zircon ages continue via the Permian until the Late Triassic, Middle Jurassic and Early Cretaceous. The high-grade metamorphic rocks of the Asterousia crystalline complex are likely equivalents of the low-grade metamorphic trench and fore-arc deposits of the Vatos nappe pointing to Late Cretaceous slab roll back. The presence of both late Permian detrital zircons and Late Cretaceous arc-type granitoids suggest that the Uppermost Unit of Crete is derived from the late Permian/Late Cretaceous magmatic belt situated north of the Sava–Vardar–Izmir–Ankara Suture in the Strandja–Rhodope area. To achieve their recent position on Crete, the nappes had to travel more than 500 km. The traveling path is well tracked by rocks of the Upper Cycladic Unit, which are similar to those of the Uppermost Unit of Crete. The large displacement of the Cretan nappes was controlled not only by nappe transport, but probably also by dextral strike–slip along the North Anatolian Fault Zone and related counterclockwise rotation of the Anatolian block since the Eocene.

Keywords Hellenides · Provenance analysis · U–Pb detrital zircon · Crete · Uppermost Unit

Introduction

The rocks of the eastern Mediterranean realm show evidence for Grenvillian, Cadomian, Variscan, Cimmerian, and Alpine orogenic events. During each of these events, large volumes of felsic igneous rocks developed, which commonly include magmatic and inherited zircons. After weathering and decomposition, the zircons were removed from the rock, transported and deposited in various basins as detrital zircons. Analysis of the type, composition and age of these detrital zircons help to reconstruct the positions of the different plates and nappes through time. Concerning the nappe stack of Crete, such type of provenance analysis is particularly important, as metamorphism and deformation related to the orogenic events damaged fossils and affected some of the isotopic systems, which are relevant for constraining the protolith ages of metasedimentary and metaigneous rocks. Moreover, the primary position of volcanic and sedimentary rocks was affected by thrusting and nappe emplacement due to subduction/collision and by extensional collapse of thickened crust. Consequently, there are fragments of lithosphere, the database of which is still incomplete and our understanding of its geological evolution is poor. Such fragments are present in the nappes of the Uppermost Unit of Crete (Fig. 1), which is the most enigmatic nappe stack of the eastern Mediterranean commonly attributed to the Internal Hellenides.

✉ G. Zulauf
g.zulauf@em.uni-frankfurt.de

S. O. Martha
silviu.martha@senckenberg.de

[1] Institut für Geowissenschaften, Goethe-Universität Frankfurt a.M., Altenhöferallee 1, 60438 Frankfurt, Germany

[2] Frankfurt Isotope and Element Research Center (FIERCE), Goethe-Universität Frankfurt a.M., Altenhöferallee 1, 60438 Frankfurt, Germany

[3] Senckenberg Forschungsinstitute und Naturmuseen, Senckenberganlage 25, 60325 Frankfurt, Germany

[4] Department of Geology, University of Patras, Patras, Greece

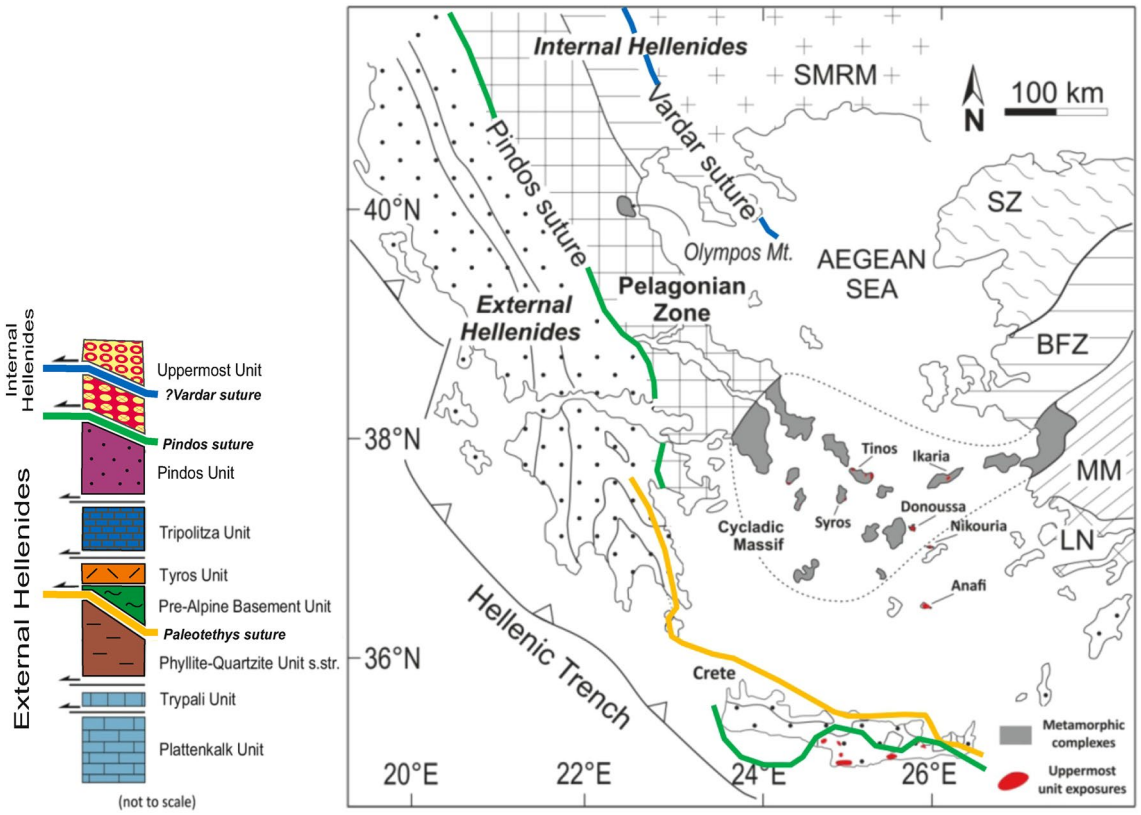

Fig. 1 Schematic sketch of the Cretan nappe stack and map of the Aegean region (modified from Chatzaras et al., 2016) showing areas of the Attico-Cycladic Massif in dark grey and exposures of Uppermost Unit in red. Exposures of Uppermost Unit after Bonneau (1972, 1984), Seidel et al. (1976, 1981), Dürr (1985), Dürr et al. (1978), Krahl et al. (1982), Reinecke et al. (1982), Thorbecke (1987), Altherr et al. (1994), Patzak et al. (1994), and Langosch et al. (2000). (BFZ, Bornova Flysch Zone; LN, Lycian Nappes; MM, Menderes Massif; SZ, Sakarya Zone; SMRM, Serbo-Macedonian and Rhodope Massifs

In contrast to the Uppermost Unit, the lower nappes of Crete (Plattenkalk, Phyllite–Quartzite s.str., Pre-Cimmerian Basement, and Tyros Unit), are part of the External Hellenides (e.g., Robertson 2012; Chatzaras et al. 2012). Detrital zircons separated from the lower nappes were investigated during several studies focusing on the closure of the Paleotethys. These studies revealed (1) a Minoan-type age spectrum characterized by a large number of Tonian/Stenian detrital zircons and a lack or only very few Mesoproterozoic zircons, apart from Stenian (Keay and Lister 2002; Zulauf et al. 2007, 2015; Marsellos et al. 2012; Dörr et al. 2015), and (2) Variscan to Cimmerian docking of microplates along the southern margin of Laurasia (Chatzaras et al. 2012; Zulauf et al. 2015, 2018, 2019). Moreover, the rocks deposited along the northern margin of Gondwana are largely free of Cambrian granite and Paleozoic detrital zircons, whereas those deposited along the southern active margin of Laurasia show evidence for early Paleozoic and Carboniferous to early Permian magmatism.

While the closure of the Paleotethys is relatively well constrained, there is still little consensus on the regional plate tectonic development during the Eohellenic (Tithonian/Early Cretaceous) and Eoalpine (Late Cretaceous) orogenic events. As no generally accepted geodynamic model exists for this period, examination of the regional geology based on field evidence is required. Defining the original provenance of the individual nappes of the Uppermost Unit of Crete remains the major tool in unraveling their movement and emplacement within the present nappe stack. Although paleomagnetic studies can be used to show how the continental separation between Gondwana and Eurasia has evolved through time (e.g., van Hinsbergen and Schmid 2012), there are still different opinions concerning the location and movement of intervening microplates. The most disputable topics are (1) the location and polarity of subduction of the Vardar lithosphere (Fig. 1), (2) the position of the individual nappe complexes of the Internal Hellenides, and (3) the provenance, movement and emplacement of those rocks, which are today forming the nappes of the Uppermost Unit.

In the present contribution, we present new U–Pb ages of zircons, which have been separated from metasediments and metaigneous rocks of the Uppermost Unit of Crete (Fig. 2a).

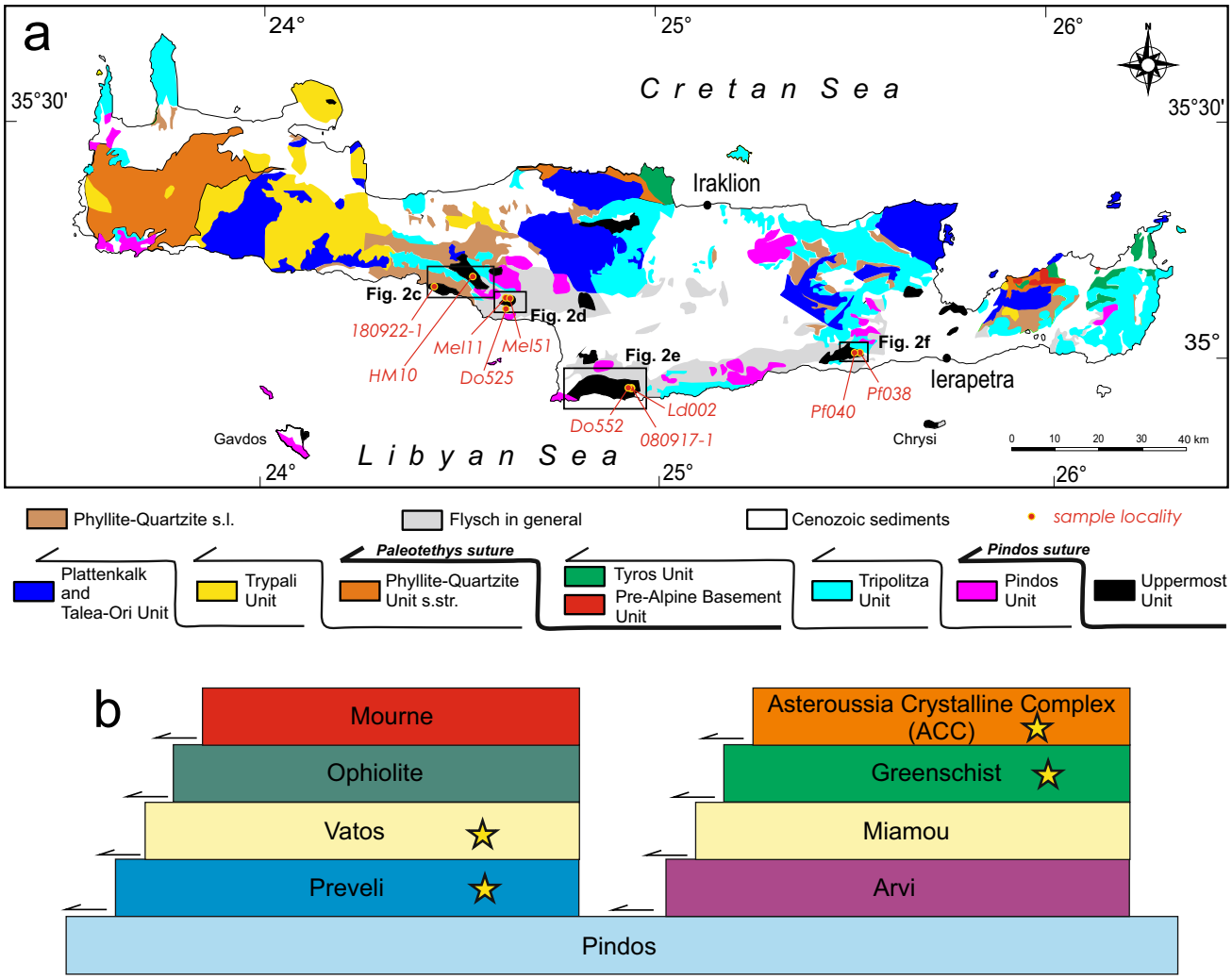

Unit/nappe	Protolith age	Type Metamorphism	Age Metamorphism
ACC	?	Amphibolite-Granulite (2)	Campanian (2, 4, 5)
Greenschist	?	Greenschist (1, 4))	Paleocene (1)
Miamou	Kimmeridgian (15)	Greenschist (15)	?
Arvi	Upper Cretaceous (16, 17)	Prehnite-Pumpellyte (16, 17)	?
Mourne	?	Blueschist/Amphibolite (3)	Upper Jurassic (3)
Ophiolite	Middle Jurassic (6)	Greenschist (10)	Upper Jurassic (9)
Vatos	Latest Jurassic - Upper Cretaceous (10, 11)	Greenschist (10, 18)	Upper Cretaceous(10)
Preveli	Late Permian - Upper Triassic (7, 8)	Epidote-Blueschist (12, 13)	Lower Cretaceous (14)

Fig. 2 **a** Map of Crete showing the different geological units (modified after Zulauf et al. 2023a, and references therein). Sample localities are indicated. **b** Nappe stacks of the Uppermost Unit resting on top of the Pindos Unit of Crete. Yellow stars indicate nappes from which samples were collected for the present study. Key to references: (1) Reinecke et al. (1982), (2) Seidel et al. (1976), (3) Seidel et al. (1977), (4) Martha et al. (2017), (5) Martha et al. (2019), (6) Liati et al. (2004), (7) Bonneau and Lys (1978), (8) Zulauf et al. (2023a), (9) Koepke et al. (2002), (10) Malten (2019), (11) Koepke (1986), (12) Koepke et al. (1997), (13) Tortorici et al. (2012), (14) Zulauf et al. in prep., (15) Bonneau et al. (1974), (16) Robert and Bonneau (1982), (17) Palamakumbura et al. (2013), and (18) Karakitzios (1988)

As in some of the investigated rocks, the temperature during Eohellenic and Eoalpine metamorphism was < 400 °C, the protolith age of sediments can be determined using fossils. Moreover, the cooling history of most of the investigated rocks is well constrained by K–Ar and ^{39}Ar–^{40}Ar ages of hornblende and white mica, and by fission-track ages of

apatite. The stratigraphy of the individual nappes of the Uppermost Unit (Bonneau and Lys 1978; Krahl et al. 1982; Zulauf et al. 2023a) provides the basis for a reasonable interpretation of the detrital zircon ages and of geological processes through time.

We will present (a) new ages of detrital zircons of metasedimentary rocks, which belong the Uppermost Unit of Crete, (b) new ages of zircons of a granitic pebble of the Pindos flysch, and (c) new ages of zircons of felsic igneous veins, which cut through high-grade metasedimentary rocks of the Uppermost Unit. The new ages, together with the shape and internal structure of the zircons, and the deformation microfabrics and composition of other detrital grains (quartz and feldspar), are used to reveal provenance areas for late Paleozoic and Mesozoic times and to reconstruct the distribution of lithospheric plates in the Eastern Mediterranean. The new ages also help to constrain the Eohellenic to Eoalpine orogenic activity within the Internal Hellenides. For simplicity, the emplacement directions of nappes or the direction of subduction are mainly referred to here in terms of modern geographical coordinates. The 2022 GSA Geologic Time Scale (http://www.geosociety.org/science/timescale/timescl.pdf) is used throughout.

Regional geology

The Uppermost Unit of Crete consists of several nappes, which are resting on top of the Pindos or on deeper units (Fig. 2a). There are two different stacks (Fig. 2b), which are briefly described in the following passages. One of these nappe stacks is exposed in central Crete in the area of Vatos–Preveli–Spili–Gerakari, near Gonies, west of Kamares, and on the island of Gavdos. This stack consists of the Preveli, Vatos, Ophiolite and Mourne nappes (Zulauf et al. 2023a, and references therein; Fig. 2a, Fig. 2c Supplement).

The *Preveli nappe* consists of Permian metasiliciclastic rocks covered by limy phyllite and middle to late Permian limestone (now marble) (Bonneau and Lys 1978), and bimodal metavolcanic rocks. The metavolcanic rocks developed in a Triassic extensional setting and led to the formation of skarn (Zulauf et al. 2023a). Towards the stratigraphic top, the mafic metavolcanic rocks dominate and are related to Upper Triassic to? Jurassic (meta)chert and cherty marble (Krahl et al. 1982). The Preveli rocks underwent Eohellenic deformation under epidote-blueschist-facies conditions at T = ca. 370 °C (Koepke et al. 1997; Tortorici et al. 2012; Zulauf et al. 2023b). Apatite fission-track ages of phyllite of the Preveli nappe are 30 ± 2 Ma (Thomson et al. 1999). The main tectonic transport during late nappe emplacement was top-to-the west.

The *Vatos nappe* (Aubouin and Dercourt 1965) consists of wildflysch-like Upper Jurassic to Upper Cretaceous metasediments and volcanics (Bonneau et al. 1977; Krahl et al. 1982; Malten 2019). Calcschists include Upper Cretaceous fossils and display a synkinematic crystallization of white mica, calcite, quartz and albite along the main foliation (Koepke 1986; Tortorici et al. 2012). Deformation microfabrics of quartz and calcite and the metamorphic index minerals, such as actinolite, chlorite, albite and white mica indicate lower greenschist-facies metamorphism (Karakitzios 1988; Malten 2019), which must be younger than Uppermost Cretaceous (the age of the fossils) but older than the Palaeocene–Eocene Pindos flysch underneath. Of particular interest are limy metaconglomerates, which include rodingite and other ophiolitic pebbles (Krahl et al. 1982) and Late Jurassic/Early Cretaceous foraminifera (Malten 2019). U–Pb dating of calcite, which precipitated in pressure shadows behind rigid clasts of the limy metaconglomerate, yielded 76 ± 4 Ma (Malten 2019), which is probably the age of the greenschist-facies metamorphism.

The *Ophiolite nappe* includes deformed metaultramafic rocks (serpentinite, metahornblendite) and meta-pillowbasalt (Krahl et al. 1982). A detailed petrographic description of the serpentinites, which are forming the basal part, is given in Koepke (1986) and Tortorici et al. (2012). Relics of spinel lherzolite result from undepleted mantle evolved along a spreading ridge with low spreading rate and deformed at very high temperature (Koepke et al. 2002). The serpentinite is overlain by metahornblendite, which was overprinted under greenschist-facies conditions. U–Pb SHRIMP dating of zircons of the metahornblendite yielded 163 ± 3 Ma, which is interpreted as crystallization age (Liati et al. 2004). K–Ar ages of hornblende yielded ca. 156 Ma (Koepke et al. 2002) meaning that the hornblendite was formed close to the Middle/Late Jurassic boundary and emplaced and cooled down to T < 500 °C still during the Late Jurassic. Gabbroic/dioritic veins, which cut through the serpentinite, yielded K–Ar hornblende ages at ca. 140 Ma, interpreted as cooling after melt emplacement (Koepke et al. 2002). The gabbroic veins were overprinted under greenschist-facies conditions at ca. 95 Ma. Younger veins of quartzdiorite and tonalite, which cut through the rocks mentioned above, are almost undeformed. One metahornblendite yielded an apatite fission-track age at 35 ± 6 Ma (Thomson et al. 1999).

The *Mourne nappe*, on top of the Ophiolite nappe, is exposed west of Mourne and between Kerames and Korifi (Fig. 2c Supplement). It consists of blueschist, amphibolite, marble and micaschist/gneiss. The blueschists contain relics of omphacite. Amphibole and phengite, separated from the crystalline rocks of Gavdos and Gerakari, yielded similar K–Ar ages at ca. 148 Ma (Seidel et al. 1977), which are compatible with the fact that the blueschists of Gavdos are unconformably overlain by Late

Cretaceous (meta)sediments (Vicente 1970; Seidel et al. 1977). Thus, similar to the Ophiolite nappe, the Mourne nappe should have been situated at upper structural levels (T < ca. 350 °C, the closure T of the K–Ar isotopic system of white mica) since the Upper Jurassic, while the Vatos Unit and the rocks of the second nappe stack (see below) underwent latest Cretaceous/Paleocene metamorphism under various conditions.

The second nappe stack consists of four subnappes, which are (from bottom to top) Arvi Unit, Miamou Unit, Greenschist Unit and Asterousia Crystalline Complex (ACC) (Fig. 2d–f Supplement). The *Arvi Unit* (Davi and Bonneau 1972; Bonneau 1973) consists of terrigenous turbidites, prehnite–pumpellyite facies metamorphic pillow basalts and reddish (meta)limestones. Maastrichtian–?Palaeocene microfossils are present in red calcareous mudstone matrix of associated lava breccia (Robert and Bonneau 1982; Papanikolaou 1989), that should have been part of an Upper Cretaceous seamount in the northern domain of the Pindos ocean (Palamakumbura et al. 2013). The *Miamou Unit* consists of flyschoid terrigenous sediments, diabase and limestones, the latter of late Jurassic age (Bonneau et al. 1974). These rocks underwent greenschist-facies metamorphism (Bonneau et al. 1974). The *Greenschist Unit* results from basic volcanic rocks with a MORB-type signature (Reinecke et al. 1982) and metasedimentary rocks. Paleocene greenschist-facies top-to-the SE displacement is documented not only on Anafi (Martha et al. 2016), but also in the Melambes and Pefkos areas of Crete (Martha et al. 2017, 2019).

The *Asterousia Crystalline Complex (ACC)* consists of high-grade metamorphic rocks (largely metasediments) and metagranitoids (Bonneau 1972; Davi and Bonneau 1972; Seidel et al. 1976, 1981; Langosch et al. 2000; Martha et al. 2019), which reflect a Late Cretaceous magmatic arc. Apart from Crete, ACC-type rocks are further present in the Upper Cycladic Unit such as Anafi, Donoussa, Nikouria, Syros, and Tinos (Fig. 1). Conditions of the low-pressure/high-temperature metamorphism of the ACC of Crete have been constrained at P = 400–500 MPa and T_{max} = 700 °C (Seidel et al. 1981). Slices of serpentinite have been incorporated into the metasedimentary rocks prior to amphibolite facies metamorphism (Bonneau 1973; Reinecke et al. 1982; Be'eri-Shlevin et al. 2009), while a large number of I-type granitoids intruded the metasedimentary successions of Anafi, western Asterousia, Melambes, and Pachia Amos during a short period in the middle to late Campanian (78–72 Ma; U–Pb on zircon, Kneuker et al. 2015; Martha et al. 2016, 2017, 2019). K–Ar biotite and hornblende ages of Cretan ACC-type rocks range from 76 to 66 Ma, and apatite fission-track ages of the ACC of Lentas range from 31 to 20 Ma (Thomson et al. 1998).

Analytical techniques

Laser ablation-inductively coupled plasma-mass spectroscopy

Samples of metasedimentary rocks collected for isotope mass spectrometry were processed at the *Institut für Geowissenschaften* of Frankfurt University using standard mineral separation techniques. These include crushing and sieving, before concentration of heavy minerals by heavy liquids (bromoform, methyleniodide) and magnetic-separation with a Frantz isodynamic separator. Hand-picked detrital zircon grains were mounted in 25-mm-diameter circular epoxy mounts and polished to expose a section at their inner core. Prior to their analysis, the grains were examined using cathodoluminescence (CL) imaging in order to reveal their internal structure and to identify cracks and mineral inclusions. U–Pb isotope analysis of detrital zircons was performed by laser ablation-inductively coupled plasma-mass spectroscopy (LA-ICPMS) using a Thermo-Finnigan Element II sector field ICPMS attached to a New Wave LUV213 laser ablation system (λ = 213 nm). Ablation was carried out in a He carrier gas in a low volume (2.5 cm^3) cell; laser beam parameters used were 30 µm diameter; 5 Hz repetition rate 75% power output. Isotope data were acquired in peak-jumping mode. Background and ablation data for each analysis were collected over 90 s, with background measurements (carrier gas, no ablation) being taken over the first 30 s prior to initiation of ablation. Data were collected at time-resolved mode allowing acquisition of the signal as a function of time (ablation depth), and subsequently recognition of isotopic heterogeneities within the ablated volume. Raw data were processed offline using an Excel® spreadsheet program created by A. Gerdes. Mass discrimination of the MS, and elemental fractionation during laser ablation were corrected by calibration against the GJ-1 zircon standard (Jackson et al. 2004), which was analyzed routinely during analytical sessions (three standard analysis at the beginning and end of every session of 33 unknowns, and 2 standard analyses every 10 unknowns). Prior to this correction, the change of elemental fractionation (e.g., Pb/U and Pb/Th ratios as function of ablation time and thus depth) was corrected for each set of isotope ratios by applying a linear regression through all measured ratios versus time, excluding some outliers (> 2 s.e.), and taking the intercept t = 0 as the correct ratio. Changes in isotopic ratios arising from laser drilling into domains of distinct Pb/U ratio (core/rim), mineral inclusions, and zones affected by Pb loss (metamictization/cracks), can usually be detected by careful monitoring of the time-resolved signal, such analyses are normally

rejected. Common Pb correction was applied only when the interference- and background-corrected ^{204}Pb signal was significantly higher than the detection limit of about 20 cps. The latter is limited by the amount of Hg in the carrier gas and the accuracy to which the ^{202}Hg and thus the interfering ^{204}Hg can be monitored. Corrections made were based on common Pb composition given by the second stage growth curve of Stacey and Kramers (1975) for Neoproterozoic age (600 Ma). Data presentation was made with Isoplot (Ludwig 1994).

Isotope dilution thermal ionization mass spectrometry

Zircon grains with the size of 100–200 µm were hand-picked from the > 1.6 Amp fraction of the heavy mineral separates for the isotope dilution thermal ionization mass spectrometry (ID-TIMS). As the ID-TIMS ages of zircons are more precise than the ages obtained using LA-ICPMS, this method was applied for determining emplacement ages for the igneous rocks. After washing with 6 N HCl and acetone, zircon grains were weighted, transferred to small Savillex beakers and put with 24 N HF for 6 h on the hotplate at 90 °C. The HF was decanted and the vials were loaded again with 24 N HF and a mixed ^{205}Pb/^{235}U spike. The small Savillex vials were then placed into a Parr bomb. After dissolution at 180 °C for 96 h and subsequent evaporation to dryness at ca. 80 °C on a hotplate, the sample was converted into chloride by adding 0.2 ml 3 N HCl. Chemical separation of Pb and U on 100 µl columns (ion-exchange resin AG 1 × 8, 100–200 mesh) followed the method of Krogh (1973). The U and Pb isotope ratios of zircon were obtained using a Finnigan MAT 261 mass spectrometer in static multicollector mode with simultaneous ion counting of ^{204}Pb. All isotopic ratios were corrected for mass fractionation (1.0 ± 0.3‰/a.m.u), blank (ca. 5 pg) and initial lead using the Stacey and Kramers (1975) model Pb composition. The Pb/U isotope ratios were plotted using Isoplot (Ludwig 2001), with error ellipses reflecting 2σ uncertainty. To verify the complete analytical procedure, standard zircons 91,500, Gj 1 and M257 have been reproduced (see data of the *Institut für Geowissenschaften* of Frankfurt University in Nasdala et al. 2008).

Microfabrics

All investigated samples underwent deformation and metamorphism. Thin sections from the samples were investigated to reconstruct the kinematics, the deformation–crystallization relations, and the deformation mechanisms of quartz and feldspar. In addition to metamorphic index minerals, the latter were used to estimate the metamorphic conditions.

Results

Locality, petrography and microfabrics of studied samples

Metasedimentary rocks

Sample 180922-1 is a fine-grained siliciclastic metaconglomerate of the basal part of the Preveli nappe, exposed 800 m SW of Lefkogia in central Crete (Fig. 2a, Fig. 2c Supplement, Table 1 Supplement). The rock is well foliated. Displaced quartz veins indicate a top-to-the SE sense of shear. Main constituents are quartz, plagioclase, K-feldspar, white mica, chlorite and opaque phases (Figs. 3a, 4a). Quartz is present in form of clasts and as newly grown fibers in pressure shadows behind rigid clasts. The clasts show evidence for both ductile and brittle deformation. Ductile deformation is weak and documented by undulatory extinction and subgrains. Serrated grain boundaries are present in both rigid clasts and newly grown quartz fibers. The quartz clasts, on the other hand, show various types of inherited fabrics including recrystallized fabrics with strikingly different grain size and chessboard-like subgrains. Exsolution of perthite lamellae in K-feldspar is also regarded as an inherited fabric (Fig. 4a).

Sample HM10 is a quartzite of the Vatos flysch exposed W of Ardaktos in central Crete (Fig. 2a, c Supplement, Table 1 Supplement). The quartzite forms the Uppermost part of this flysch sequence (Fig. 3b) and displays primary bedding in form of light and dark layers (Fig. 3c). The bedding plane dips moderately towards NNE. The quartzite is cut by a subhorizontal brittle shear plane, which shows a N–S trending striation. The quartzite results from badly sorted sandstone. Apart from quartz, there are other components such as white mica, plagioclase, chlorite and opaque phases. The large quartz grains show evidence for deformation portrayed by serrated grain boundaries and stylolites (Fig. 4b), which indicate both dislocation and dissolution–precipitation creep as the main deformation mechanisms. Inherited fabrics are similar to those described from sample 180922-1.

Sample Mel11 is made of quartzite of the Greenschist Unit exposed 1.5 km SW of Nea Krya Vrysi (Melambes area, central Crete, Fig. 2a, d Supplement, Table 1 Supplement). The quartzite is impure and consists of ca. 75% of quartz and minor amounts of garnet, K-feldspar, plagioclase, white mica, clay minerals and accessories. Quartz shows a very fine-grained dynamically recrystallized fabric. Relics of small, elongated older grains display undulatory extinction and subgrains. Similar to the micas, most of the quartz grains show a weak shape-preferred orientation. Garnet was largely replaced by

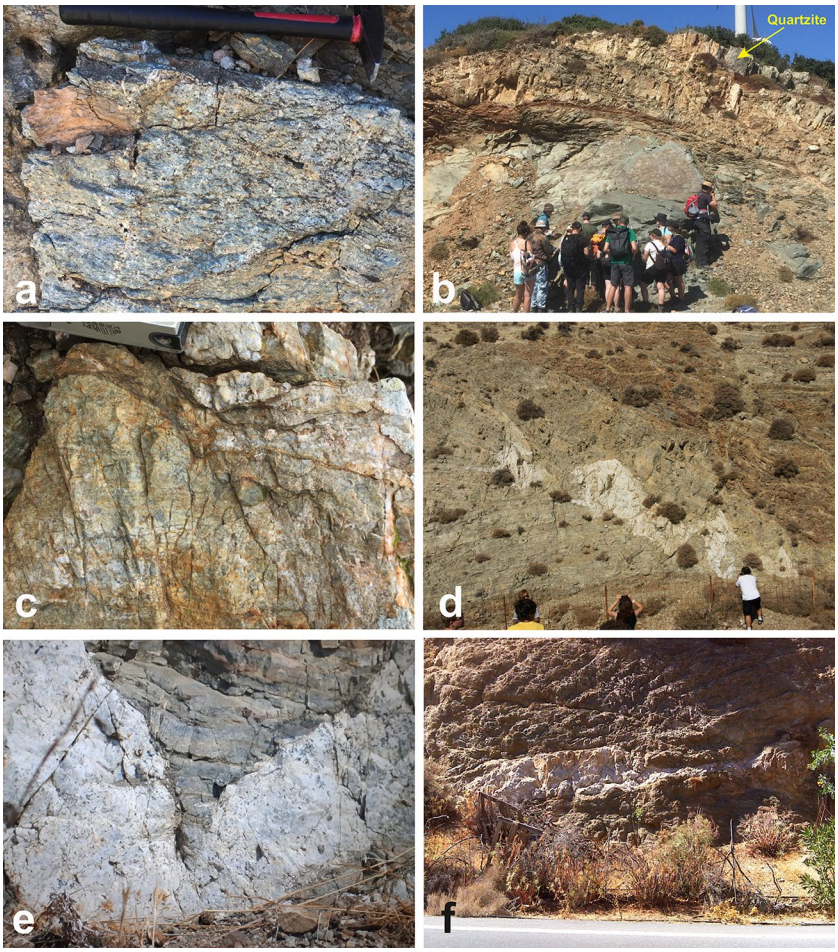

Fig. 3 Field photographs of studied rocks. **a** Siliciclastic metaconglomerate of the Preveli nappe exposed SW of Lefkogia (sample 180922–1); view is subparallel to the WNW–ESE trending stretching lineation; length of hammer = 28 cm. **b** Vatos wildflysch exposed WSW of Ardaktos showing quartzite layer at the top, from which sample HM10 was collected. **c** Detail of quartzite (sample HM10); length of compass = 9 cm. **d** Discordant folded granitic vein (sample 0909–17-1) in quartzite of the Asterousia Crystalline Complex (ACC) is cut by normal faults; road cut between Krotos and Lentas. **e** Close-up view of contact between fold hinge of granitic vein and greyish foliated quartzite (sample Do552); same locality like in (**d**). **f** Boudinaged granitic vein (sample Ld002) in metasediments of the ACC; road cut between Krotos and Lentas

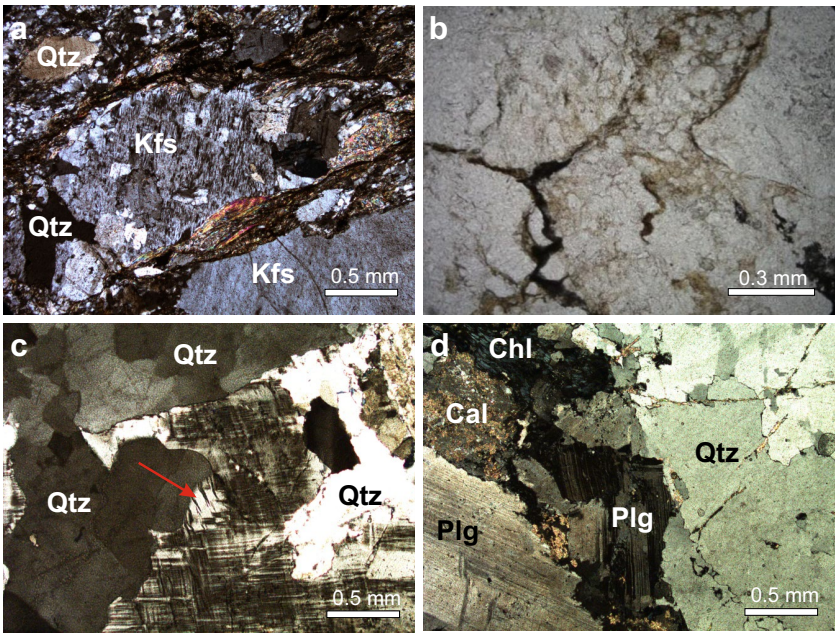

Fig. 4 Microphotographs of investigated rocks. **a** Metaconglomerate of basal Preveli nappe with large amount of detrital feldspar (180922–1, SW of Lefkogia). **b** Quartzite of Vatos flysch showing evidence for dissolution–precipitation creep in form of dark stylolites (HM 10, W of Ardaktos). **c** High-temperature deformation of granitic vein is indicated by chessboard-like subgrains in quartz, formation of myrmekite (red arrow), and sutured phase boundaries (080917–1, road cut between Lentas and Krotos). **d** Red granite of Pindos flysch (Do525, W of Melambes). Ductile deformation is indicated by serrated grain boundaries of quartz and deformation twins in plagioclase

chlorite. Further details concerning the content and texture of this quartzite are described in Martha et al. (2017).

Sample Mel51 consists of quartzite collected from the ACC 1 km SSE of Nea Krya Vrysi (Melambes area, central Crete, Fig. 2a, d Supplement, Table 1 Supplement). The quartzite consists of quartz, K-feldspar, plagioclase, garnet, biotite, epidote, white mica and chlorite. The fabric of quartzite is mylonitic with ribbons of quartz and mineral clasts in a fine-grained, dynamically recrystallized matrix consisting mostly of quartz. A striking foliation results from almost pure layers of recrystallized quartz in alternation with impure layers. For further details of this rock, see Martha et al. (2017).

Sample Pf038 is a quartzite of the ACC exposed in Sykologos village (Pefkos area of eastern Crete, Fig. 2a, f Supplement, Table 1 Supplement). Quartzite is impure and consists of > 75% of quartz, with diopside, biotite, white mica, clay minerals and opaque phases as accessories. Quartz shows an equilibrium fabric (foam structure) of polygonal and small grains with few larger elongated grains forming clusters or thin layers. The grain size of quartz is correlated with the amount of impurities, quartz grains being larger in almost pure layers. The shape-preferred orientation of quartz in quartzite is supported by the grain-shape fabrics of biotite and clay minerals. For further details, see Martha et al. (2019).

Sample Pf040 consists of chiastolite hornfels of the ACC, which has been collected 200 m SE of Ag. Georgios (Pefkos area of eastern Crete, Fig. 2a, f Supplement, Table 1 Supplement). The chiastolite hornfels consists of quartz, biotite, plagioclase, andalusite, K-feldspar, white mica, garnet, chlorite, clay minerals and graphite (Martha et al. 2019). Quartz is present in form of fine-grained recrystallized matrix and aggregates of large recrystallized grains. Quartz shows weakly developed chessboard patterns based on prism- and basal-parallel subgrains. Biotite inclusions and pinning of quartz grain boundaries by biotite are common. K-feldspar shows undulatory extinction, while Karlsbad twinning is rare. Garnet may occur as euhedral porphyroblasts or is anhedral in layers. Garnet porphyroblasts are strongly disintegrated and were partly replaced by white mica, chlorite and clay minerals. For further details of this rock, see Martha et al. (2019).

Sample Do552 is a quartzite of the ACC exposed between Krotos and Lentas (central Crete, Fig. 2a, e Supplement, Table 1 Supplement). The grey quartzite is well foliated (Fig. 3e) and intercalated with biotite schist and paragneiss. Quartz of the quartzite displays a pervasively recrystallized fabric. This sequence is cut by granitic veins described below (Fig. 3d–f).

Meta-igneous rocks

Sample 080917–1 was collected from a granitic dike, which cuts through metasediments of the ACC between Krotos and Lentas (Fig. 2a, e Supplement, Table 1 Supplement). The thickness of the vein varies from 50 cm to ca. 2 m. Macroscopic deformation of the vein is indicated by open to tight folds (Fig. 3e) and by normal faults (Fig. 3d). Constituent minerals of the vein are quartz, K-feldspar, plagioclase and minor biotite, which is partly replaced by chlorite. Although the vein is free from foliation, it shows evidence for ductile deformation. The original quartz grains were up to 1 cm in diameter. Ductile deformation of quartz was accommodated by recrystallization driven by strain-induced grain boundary migration, which led to grain-size reduction. High-temperature deformation is indicated by chessboard-type subgrains in quartz and by serrated phase boundaries between quartz and K-feldspar (Fig. 4c). K-feldspar is present in form of microcline, which is up to 2 cm in diameter and shows flame perthite and replacement by myrmekite. K-feldspar is partly recrystallized along discrete planes, which show newly grown tiny crystals. Plagioclase is up to 5 cm in diameter. Some crystals show primary zonation and inclusions of white mica.

Sample Ld002 was collected from a granitic sill, which is aligned subparallel to the foliation of the ACC metasediments cropping out between Krotos and Lentas (Fig. 2a, e Supplement, Table 1 Supplement). The sill is similar in composition and deformation microfabrics like the dike described above from sample 080917-1 but includes a large number of titanite, which is up to 300 µm in size. Moreover, the macroscopic deformation is portrayed by boudinage, which reflects extension subparallel to the foliation of the wall rock (Fig. 3f).

Sample Do525 was collected from a reddish granite pebble that is several meters in diameter and part of the Pindos flysch exposed along a field path W of Melambes (Fig. 2a, d Supplement, Table 1 Supplement). The granite consists of quartz, plagioclase, K-feldspar and chlorite. Quartz is up to 8 mm in diameter. Apart from young fractures, there is evidence for earlier high-temperature deformation in form of serrated grain boundaries and chessboard-type subgrains in quartz (Fig. 4d). Plagioclase is up to 4 mm in diameter and shows striking deformation twins after the albite and pericline law. The twin lamellae are often bent or kinked. K-feldspar is up to 6 mm in diameter and affected by sericitization. Both plagioclase and K-feldspar are reddish and partly replaced by calcite, which is affected by a large number of type 2 twins (after Burkhard 1993). Twinned calcite is also present along fractures. The serrated phase boundaries between quartz and plagioclase and between plagioclase and K-feldspar are further evidence for high-temperature

deformation. Chlorite is up to 4 mm long and seems to have developed by replacement of former biotite.

U–Pb zircon data

Metasedimentary rocks

Siliciclastic metaconglomerate of Preveli Unit (sample 180922-1) Fifty-four zircons have been separated from the Preveli metaconglomerate sample 180922-1. The zircons vary significantly in size and in shape. The largest zircon is 250 µm in diameter. Most zircons are well rounded to subrounded and display a striking oscillatory zonation in CL images (Fig. 5a). There are up to three growth stages. Some of the zircons are pitted or fractured, and only few are euhedral in shape.

Only few zircons are older than Ediacaran (Fig. 6a, b, Table 2 Supplement). They include Tonian/Stenian as well as Paleoproterozoic and Neoarchean ages. Eight zircons are Ediacaran and 13 zircons are Cambrian–Ordovician in age. The rest of the zircons are Carboniferous with peaks at 351 ± 3 Ma, 337 ± 2 Ma and 319 ± 3 Ma. The youngest zircon is 305 ± 6 Ma.

Quartzite of Vatos flysch (sample HM10) Fifty zircons have been separated from the quartzite sample HM10. The size of the zircons varies from 40 to 200 µm. The shape and structure of the zircons is similar to those described from sample 180922-1. Most zircons are well rounded to subrounded and display a striking oscillatory zonation in CL images (Fig. 5b). The number of fractured zircons is high, and only few are euhedral.

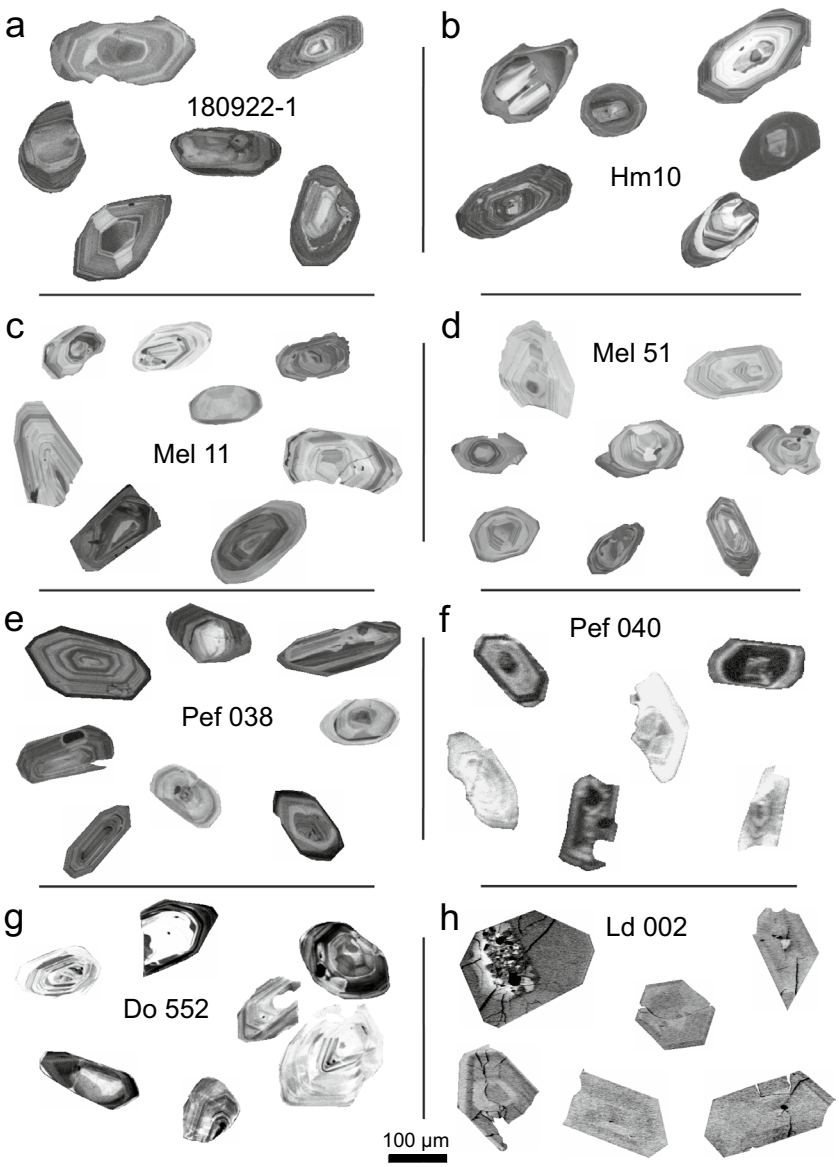

Fig. 5 CL images of selected zircon grains

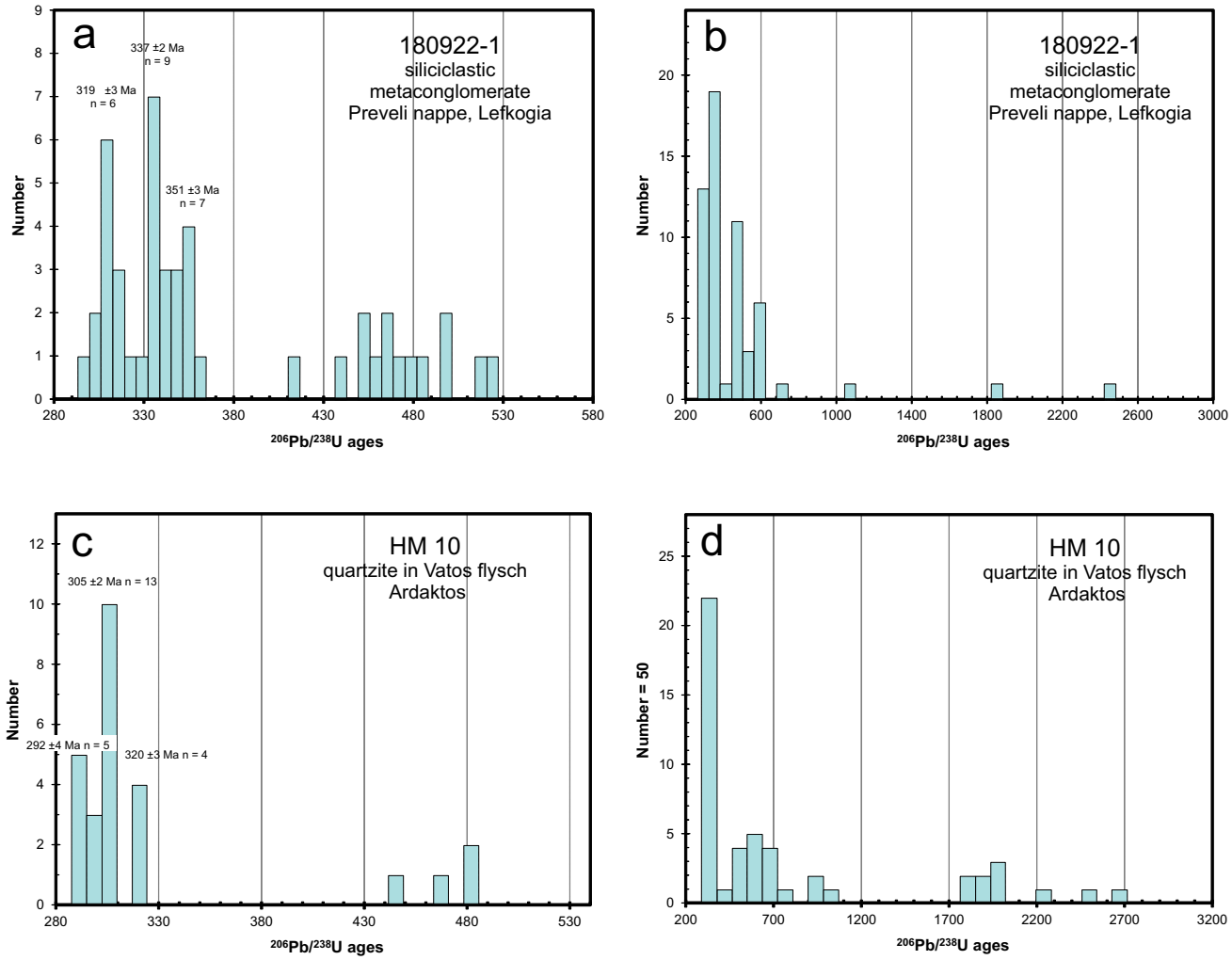

Fig. 6 Density plots of detrital zircons of Permian siliciclastic metaconglomerate of the Preveli nappe (**a**, **b**), and of quartzite of the Vatos flysch (**c**, **d**). Note the different scales of the horizontal axes

Nine zircons are Paleoproterozoic in age (Fig. 6c, d, Table 3 Supplement). Apart from Stenian types, Mesoproterozoic zircons are lacking. Four zircons are Tonian, four are Cryogenian, and 5 are Ediacaran in age. The number of early Paleozoic (Cambrian–Ordovician) zircons is very low. Most of the zircons are Carboniferous to early Permian, with peaks at 320 ± 3 Ma, 305 ± 2 Ma and 292 ± 4 Ma (Fig. 6c). The youngest zircon is 289 ± 6 Ma.

Quartzite of greenschist unit (sample Mel11) Seventy-four zircons have been separated from the quartzite sample Mel11. The size of the zircons varies from 70 to 250 µm. About a quarter of the zircons is euhedral with slightly rounded edges. The other zircons are subrounded to well rounded. Most of the zircons display a striking oscillatory zoning (Fig. 5c). Some zircons are fractured. The zoning of the zircons reflects up to three growth stages. Few zircons show holes in the central part or along the margin.

Only 15% of the zircons are older than 1 Ga, two of which are Archean, seven are Neoproterozoic and further two are Mesoproterozoic (Fig. 7a,b, Table 4 Supplement). Eleven zircons are Ediacaran with peaks at 575 ± 5 Ma and 544 ± 6 Ma (Fig. 7a). Cambrian zircons are lacking and two are Ordovician in age. Devonian and early Carboniferous zircons are also scarce. Most zircon ages are straddling the Carboniferous/Permian boundary with a small peak at 303 ± 3 Ma and the most important peak at 291 ± 2 Ma (Fig. 7a). The middle and late Permian period is also reflected by the zircon ages with a peak at 273 ± 2 Ma. Triassic zircons are also present with a Norian peak at 214 ± 2 Ma. The youngest detrital zircon is Late Jurassic (157 ± 4 Ma, Table 4 Supplement).

Quartzites of Asterousia Crystalline Complex The preparation of *sample Do552* of ACC quartzite yielded 102 detrital zircons. The size of the zircons varies from 40 to 260 µm.

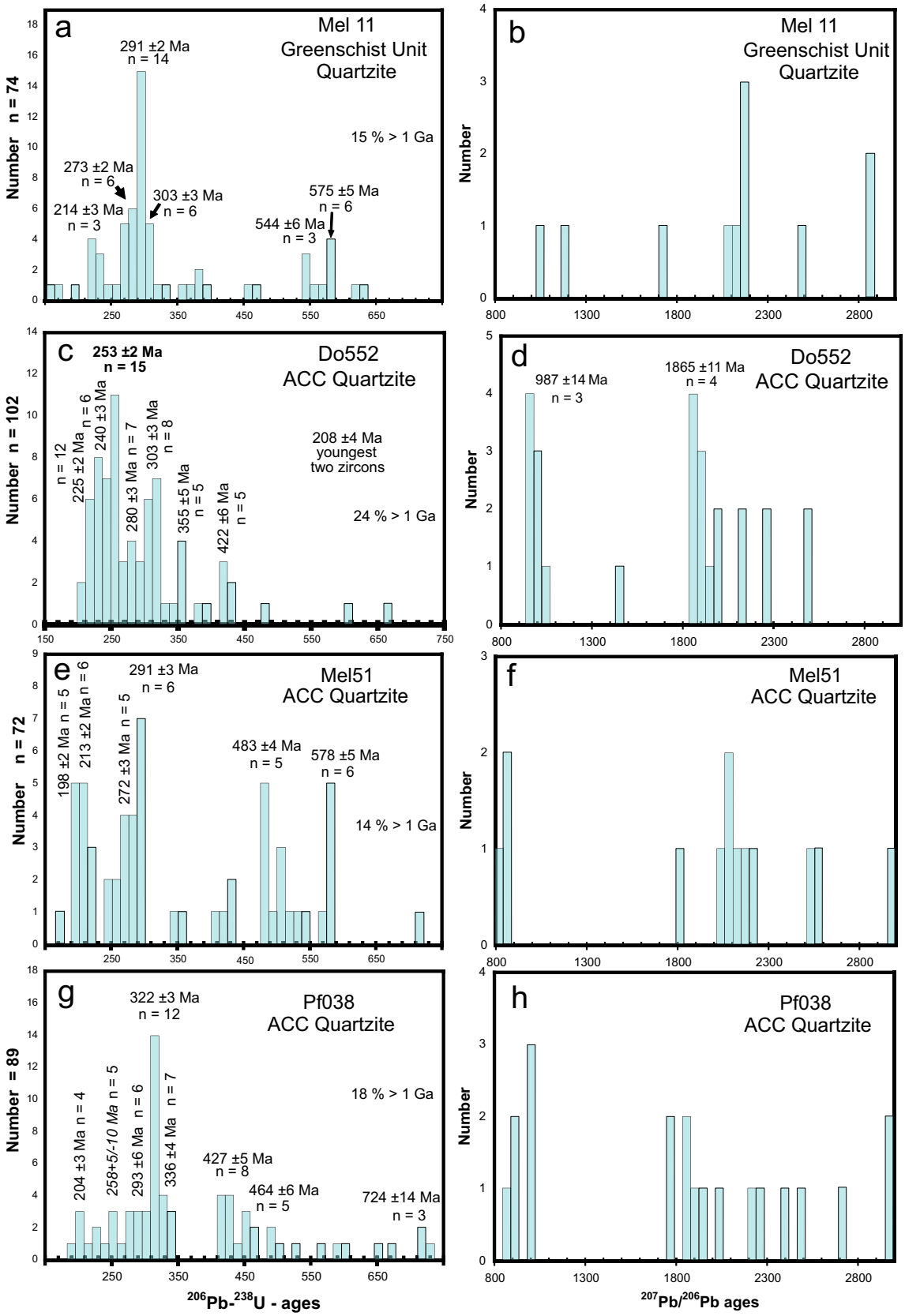

Fig. 7 Density plots of detrital zircons of quartzites of Greenschist Unit and ACC collected from the area of Melambes (**a**, **b**, **e**, **f**), Lentas-Krotos (**c**, **d**), and Pevkos (**g**, **h**). Note the different scales of the horizontal axes

Most zircons are rounded to subrounded and display a striking oscillatory zoning with up to three growth stages (Fig. 5g). Some of the zircons are pitted. A large number of zircons is present as fragments, which results from fracturing of former intact zircons.

The number of zircons > 1 Ga is low (24%, Fig. 7d, Table 5 Supplement). Most of these old zircons are Paleoproterozoic with a peak at 1865 ± 11 Ma. There is only one Mesoproterozoic zircon, while the number of Tonian zircons is high at 10, with a peak at 987 ± 14 Ma (Fig. 7d). Zircons with ages from Cryogenian to Ordovician are almost lacking. The number of Silurian zircons is elevated with a peak at 422 ± 6 Ma (Fig. 7c). The same holds for Carboniferous zircons, which display peaks at 355 ± 5 and 303 ± 3 Ma. There is an almost complete and continuous spectrum of Permian and Triassic zircons with peaks at 280 ± 3 Ma, 253 ± 2 Ma (main peak), 240 ± 3 Ma, and 225 ± 2 Ma. The youngest zircon grain is late Norian at 207 ± 6 Ma.

Seventy-two zircons have been separated from the quartzite *sample Mel51*. The zircons are similar to those described above from sample Mel11. Their size varies from 50 to 270 µm. Euhedral zircons with rounded edges are frequent. Some show sector zoning. Half of the zircons are well rounded. Most of these rounded zircons are also broken and some are pitted (Fig. 5d). The oscillatory zoning of the zircons reflects up to two growth stages.

Two zircons are Archean and 8 zircons are Paleoproterozoic (Fig. 7f, Table 6 Supplement). Four zircons are Tonian. The number of Ediacaran zircons is six with a peak at 578 ± 5 Ma (Fig. 7e). There are also Cambrian and Ordovician zircons with a peak at 483 ± 4 Ma. The number of Silurian, Devonian and Carboniferous zircons is very low. Many zircons are Permian in age, with the most important peak at 291 ± 3 Ma and a further moderate peak at 272 ± 3 Ma (Fig. 7e). Ten zircons are Triassic with a Norian peak at 213 ± 2 Ma. Six zircons are Jurassic with a Hettangian peak at 198 ± 2 Ma (Fig. 7e). The two youngest detrital zircons are Middle Jurassic (170 ± 4 Ma) and Late Cretaceous (Cenomanian, 98 ± 2 Ma).

The preparation of sample Pf038 of ACC quartzite yielded 89 detrital zircons. The size of these zircons varies from 70 to 260 µm. About half of the zircons are euhedral with slightly rounded edges (Fig. 5e). Based on their oscillatory zoning, up to two growth stages are indicated. Sector zoning is present but not common. Few zircons show striking holes. The other zircons are subrounded to well rounded. The zoning of these zircons reflects up to four growth stages.

The number of zircons older than 1 Ga is low at 18% (Fig. 7h, Table 7 Supplement). Three zircons are Archean and eleven are Paleoproterozoic. Nine zircons are Tonian with a peak at 724 ± 14 Ma. The number of Ediacaran and Cambrian zircons is low, whereas that of Ordovician and Silurian is higher with peaks at 464 ± 6 Ma and 427 ± 5 Ma, respectively (Fig. 7g). The number of Carboniferous zircons is high with a moderate peak at 336 ± 4 Ma and the most important peak at 322 ± 3 Ma. Zircons with ages throughout the entire Permian period are also present with peaks at 293 ± 6 Ma and 258 + 5/−10 Ma (Fig. 7g). Eight zircons are Triassic with a Rhaetian peak at 204 ± 3 Ma. This is the youngest age of detrital zircons of this sample.

Chiastolite hornfels of Asterousia Crystalline Complex

Preparation of the chiastolite bearing hornfels exposed near Pefkos (sample Pf040) yielded only 16 zircons, four of which with bad quality concerning age dating (concordancy < 90%, Table 8 Supplement). The size of the zircons varies from 100 to 200 µm. Only few of the zircons are euhedral and well preserved. They show oscillatory zoning. The other zircons are subrounded and are present as pitted fragments of former larger intact crystals (Fig. 5f).

As many granitoids of the ACC intruded at 74–75 Ma (Kneuker et al. 2015; Martha et al. 2017), and the chiastolite hornfels is clearly of contact metamorphic origin related to a non-exposed pluton, the youngest concordant zircons at 74 ± 2 Ma and 75 ± 2 Ma are interpreted as the age of contact metamorphism (Fig. 8a; Martha et al. 2019). The zircons, which are older than 75 Ma, should be of detrital origin. Apart from one Tonian zircon, there are Silurian and Devonian zircons with a peak at 408 ± 14 Ma (Fig. 8a). Carboniferous zircons are lacking, whereas Permian zircons are present at 270 ± 8 Ma, 262 ± 8 Ma, and 253 ± 4 Ma (Fig. 8a, Table 8 Supplement). The youngest detrital zircon with a reliable age is Middle Jurassic (167 ± 5 Ma). There is one zircon with an age at 82 ± 3 Ma, which, however, displays a low degree of concordance (84%, Table 8 Supplement).

Igneous rocks

Reddish granite boulder in Pindos flysch Preparation of the reddish granite boulder (sample Do525) yielded 30 zircons, which are largely euhedral. The size of the zircons is up to 180 µm. Most of the zircons show up to 7 holes. Some are strongly resorbed along the margins, while other zircons are fractured. Based on the oscillatory zoning, two growth stages are inferred. Two of the zircons are two small and could not be used for age dating. The seven youngest zircons yielded a concordia age at 234 ± 2 Ma, which is interpreted as the emplacement age of the granite (Fig. 8b). Inherited zircons yielded ages at 245 ± 6, 246 ± 6, 262 ± 7 and 271 ± 7 Ma (Table 9 Supplement).

Granitoid veins in Asterousia Crystalline Complex Six euhedral zircons have been separated from a granitoid dike, which cuts through quartzite of the ACC near Lentas (sample 080917-1). These zircons are similar to those of

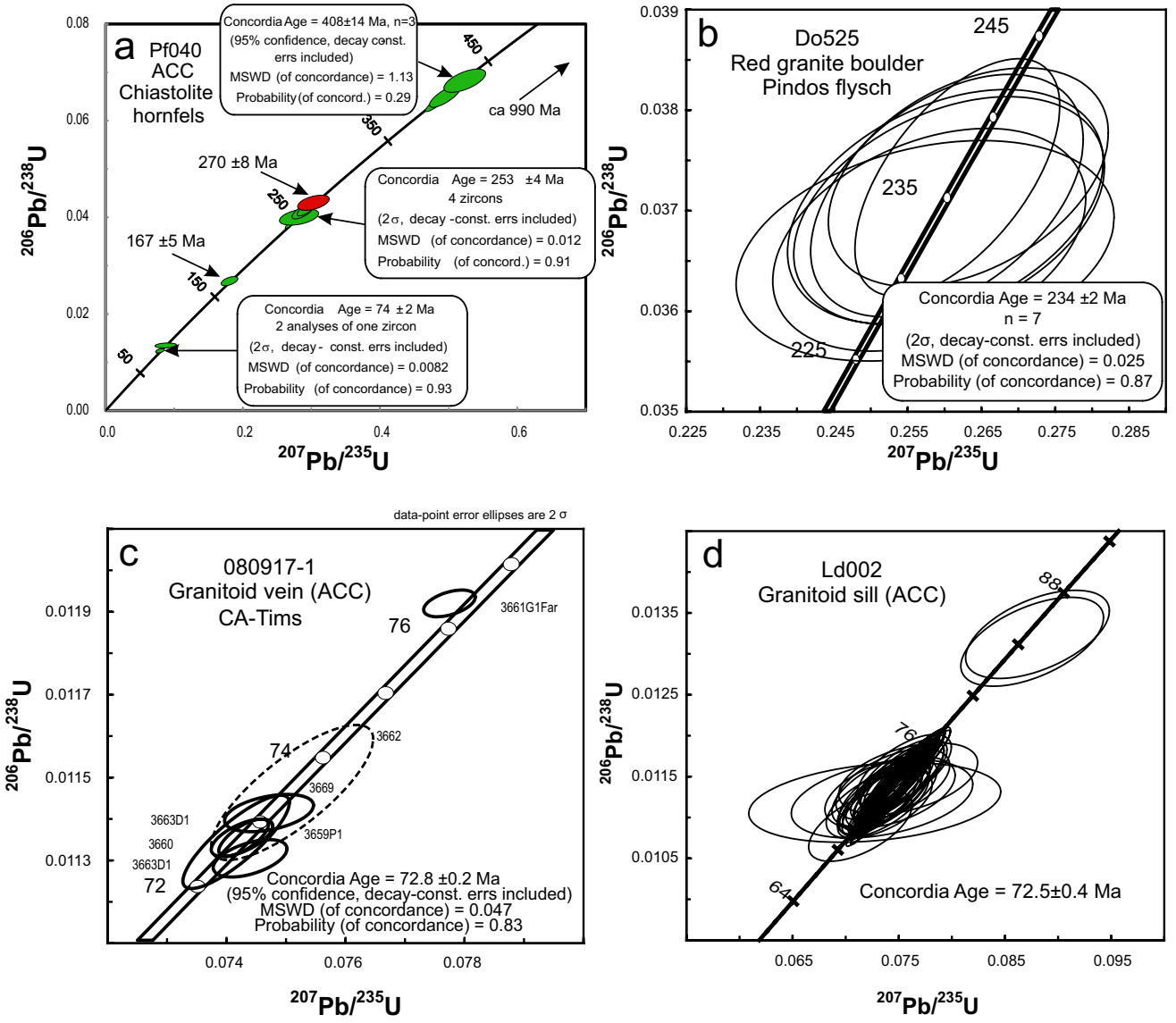

Fig. 8 U–Pb concordia plot of analyzed zircons of chiastolite hornfels of ACC (**a**), of granite boulder in Pindos flysch (**b**), and of granitoid veins of ACC (**c**, **d**)

the granitoid sill described below. Their size varies from 100 to 350 µm, and only one growth stage is documented. The zircons yielded a concordia age at 72.8 ± 0.2 Ma (Fig. 8c, Table 10 Supplement). This age is interpreted as emplacement age of the melt.

Preparation of a granitoid sill (sample Ld002) yielded 70 zircons. The size of the zircons varies from 50 to 300 µm. All of the zircons are euhedral, but in most cases fractured (Fig. 5h). Four of the zircons are of bad quality concerning age dating and thus were not considered (Table 11 Supplement). The other zircons yielded a concordia age at 72.5 ± 0.4 Ma (Fig. 8d), which should reflect the time of melt emplacement.

Discussion

Provenance of the Vatos and Preveli Unit

Inherited deformation microfabrics of detrital grains, such as quartz or feldspar, are well preserved in the Preveli metaconglomerate and in the Vatos quartzite, because the temperature during metamorphism was low (< 400 °C, see references above). The inherited fabrics of detrital quartz and feldspar grains of the Preveli metaconglomerate and of the Vatos quartzite unequivocally indicate high-grade metamorphic rocks in the source areas. This holds particularly

for the exsolution of perthite lamellae in K-feldspar and for the chessboard pattern in quartz. This type of subgrains results from the combination of prism- and basal-parallel subgrains, which develop at $T > 600$ °C in the stability field of high-quartz (Mainprice et al. 1986; Kruhl 1996).

The depositional age of the Preveli metaconglomerate is constrained to the early/middle Permian based on the age of the youngest detrital zircon (latest Carboniferous, 305 ± 6 Ma) and the middle to late Permian age of the Preveli marble on top (Bonneau and Lys 1978). Because of the large amount of Carboniferous detrital zircons and the high-grade metamorphic inherited fabrics of detrital quartz and feldspar, the Preveli metaconglomerate and related siliciclastic rocks are regarded as Variscan molasse. The entire detrital zircon age spectrum of the Preveli metaconglomerate, with a clear dominance of Carboniferous zircons, few Silurian and Cambro-Ordovician zircons, an Ediacaran age peak, the presence of Tonian/Stenian zircons and a Mesoproterozoic age gap (Fig. 9), is similar to the detrital zircon age spectrum of the pre-Cimmerian basement and of the Tyros Unit of the lower nappes, which are part of the External Hellenides (Zulauf et al. 2015, 2018; Chatzaras et al. 2012).

The Ediacaran detrital zircons should be derived from felsic magmatic rocks, which emplaced during the assembly of northeastern Gondwana (e.g., Abdelsalam et al. 2002; Kröner and Stern 2005; Küster et al. 2008). Tonian/Stenian zircons and a Mesoproterozoic age gap are characteristic for northeast Gondwana and related Minoan Terranes (Avigad et al. 2003; Zulauf et al. 2007, 2015; Küster et al. 2008; Stern et al. 2010; Meinhold et al. 2013; Dörr et al. 2015). This holds particularly for the Arabian–Nubian shield (Meinhold et al. 2021), which largely comprises Neoproterozoic juvenile oceanic island arcs (e.g., Stern et al. 2010; Johnson et al. 2011). This Minoan-type age spectrum is characteristic not only for the pre-Cimmerian basement of the External Hellenides, but has also been detected in the Cyclades (e.g., Keay and Lister 2002; Löwen et al. 2015; Hinsken et al. 2015; Bröcker et al. 2016; Seman et al. 2017), western Turkey (Ustaömer et al. 2012a, b, 2016; Zlatkin et al. 2012), the Serbo-Macedonian Massif (Meinhold et al. 2010), the basement of the Pannonian Basin (Pozsgai et al. 2016), Sicily (Williams et al. 2012), Sardinia (Avigad et al. 2012), and the eastern Alps (Heinrichs et al. 2012) (see also age compilation in Fig. 13 of Dörr and Stein 2019).

The Cambrian and Ordovician detrital zircons of the Preveli metaconglomerate are probably related to igneous activity along a late Cadomian magmatic arc situated at the margin of northeastern Gondwana. Associated (meta)granitoids are today exposed in the pre-Cimmerian basement of eastern Crete (Romano et al. 2004) and on the Peloponnesus (Dörr et al. 2015). The separation of the Cambrian magmatic arc from northeastern Gondwana started with the Devonian opening of the Paleotethys (Stampfli et al. 2013). Few of the early Paleozoic detrital zircons could also be derived from the Arabian–Nubian shield, where related magmatic rocks are also exposed (Fritz et al. 2013).

Based on the youngest detrital zircon of the *Vatos quartzite* (289 ± 6 Ma), the maximum deposition age of this rock is middle Permian and thus significantly older than the Jurassic/Early Cretaceous maximum deposition age of the Vatos beds as constrained by faunal composition (Malten 2019). For this reason, our field-based assumption that the sedimentary sequence of the quartzite is part of an olistolith within the Vatos flysch, is corroborated. As the number of inherited high-grade metamorphic fabrics in the Vatos quartzite is similarly high as in the Preveli metaconglomerate, we interpret the detrital components of the Vatos quartzite to be derived also from Variscan high-grade metamorphic and igneous rocks.

As the protoliths of the Vatos Unit are consistent with the main constituents of the ACC-type rocks (see below), we regard both as equivalents, meaning that the protoliths of all these rocks were deposited in a Late Jurassic to Late Cretaceous trench to fore-arc setting and accreted to the upper plate during progressive subduction. Because of slab rollback, the arc was 'shifted' towards the accreted Vatos-type rocks, which explains their HT–LP metamorphic overprint and the intrusion of calc-alkaline plutons and veins in Campanian times.

The trench and fore-arc deposits mentioned above were deposited, while the rocks of the Preveli Unit underwent Eohellenic (Late Jurassic to Early Cretaceous) subduction and related HP–LT metamorphism (Seidel et al. 1977; Koepke et al. 1997; Zulauf et al. 2023b). The pre-Permian detrital zircons of the Preveli Unit are similar to those of the ACC and Greenschist Unit, which are characterized by Carboniferous (Variscan) ages and a Minoan-type age spectrum. A correlation of the Preveli blueschists with HP–LT rocks of Greek mainland and of adjacent domains (Seidel et al. 1977) is supported by findings of late Jurassic (Tithonian) blueschists in the Vardar Zone (Robertson 2012, and references therein), in the Pelagonian Zone (Altherr et al. 2023), and in the Strandja Massif and Circum–Rhodope Belt (Fig. 10; e.g., Okay et al. 2001; Sunal et al. 2011; Burg 2012, and references therein; Okay and Nikishin 2015; Liati et al. 2016). Moreover, the Triassic rift-related volcanic rocks of the Preveli nappe (Zulauf et al. 2023a) might form equivalents of the Triassic A-type granitoids of the Serbo-Macedonian Zone (Himmerkus et al. 2009), which also show evidence for a Eohellenic HP–LT metamorphism (Mposkos et al. 2021, and references therein).

Besides the possible source areas in northern Greece, Balkan and NW Turkey, the Preveli and Vatos rocks might have been derived from the Central Pontide Supercomplex (Fig. 10; Okay et al. 2006; Aygül et al. 2016), where Early Cretaceous eclogites and blueschists are exposed (Altherr

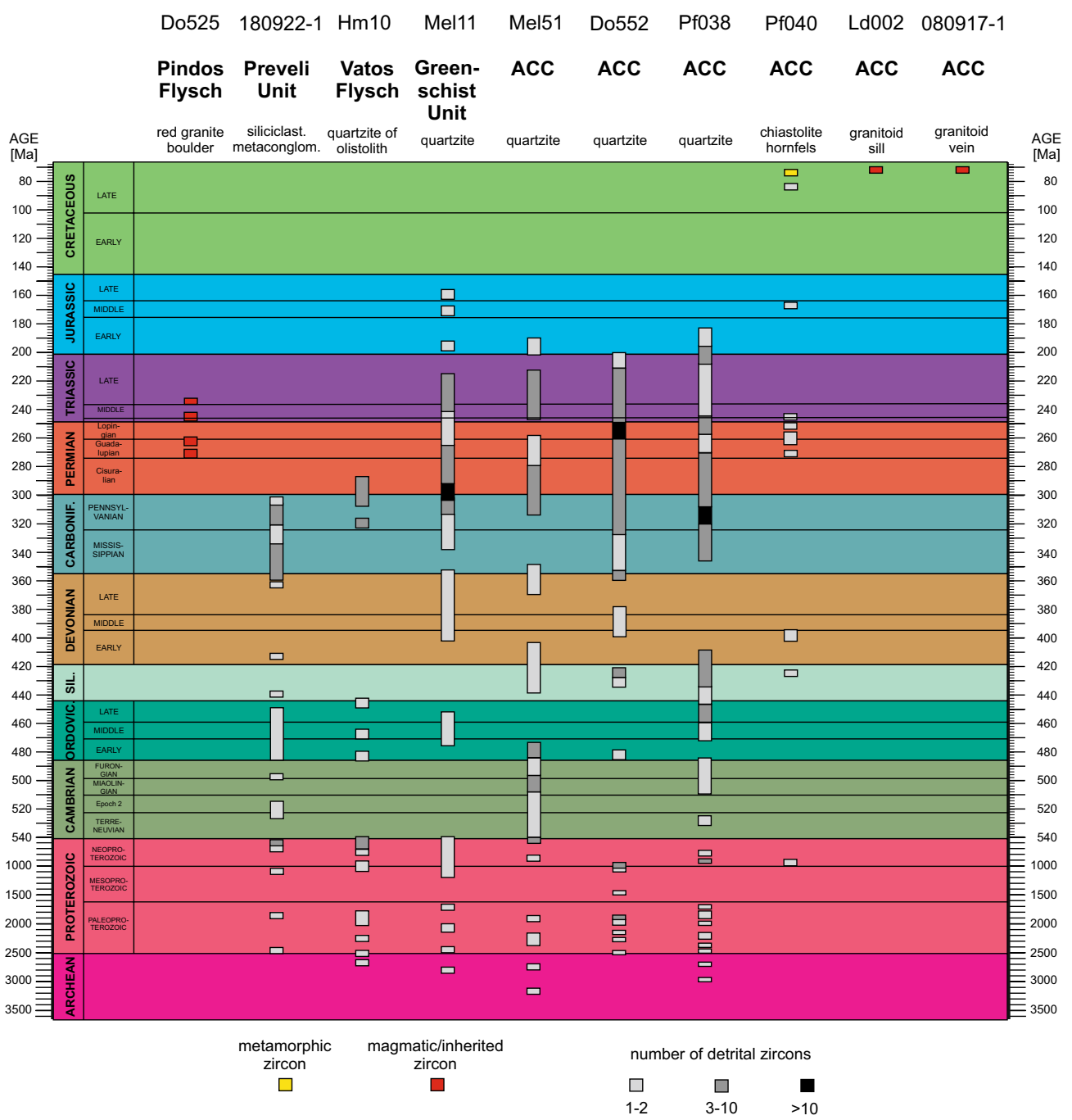

Fig. 9 Compilation of new U–Pb ages of magmatic, inherited, metamorphic and detrital zircons of the Uppermost Unit and of Pindos flysch. ACC = Asterousia Crystalline Complex

et al. 2004; Okay et al. 2006). Towards the south, a further metabasite–marble-dominated unit, characterized by Middle Jurassic blueschist-facies metamorphism, is present (Aygül et al. 2016). Possible equivalents of the Vatos rocks are exposed in the Eselner and Dady Unit (Okay et al. 2013).

The detrital zircon isotopic data of the Istanbul Zone and of the Proto-Pelagonian metasediments, on the other hand, include Mesoproterozoic zircons and a lack of Neoproterozoic zircons, pointing to an Amazonian source for these sequences (Ustaömer et al. 2011; Zlatkin et al. 2014). These areas can be ruled out as possible source for the rocks of the present study.

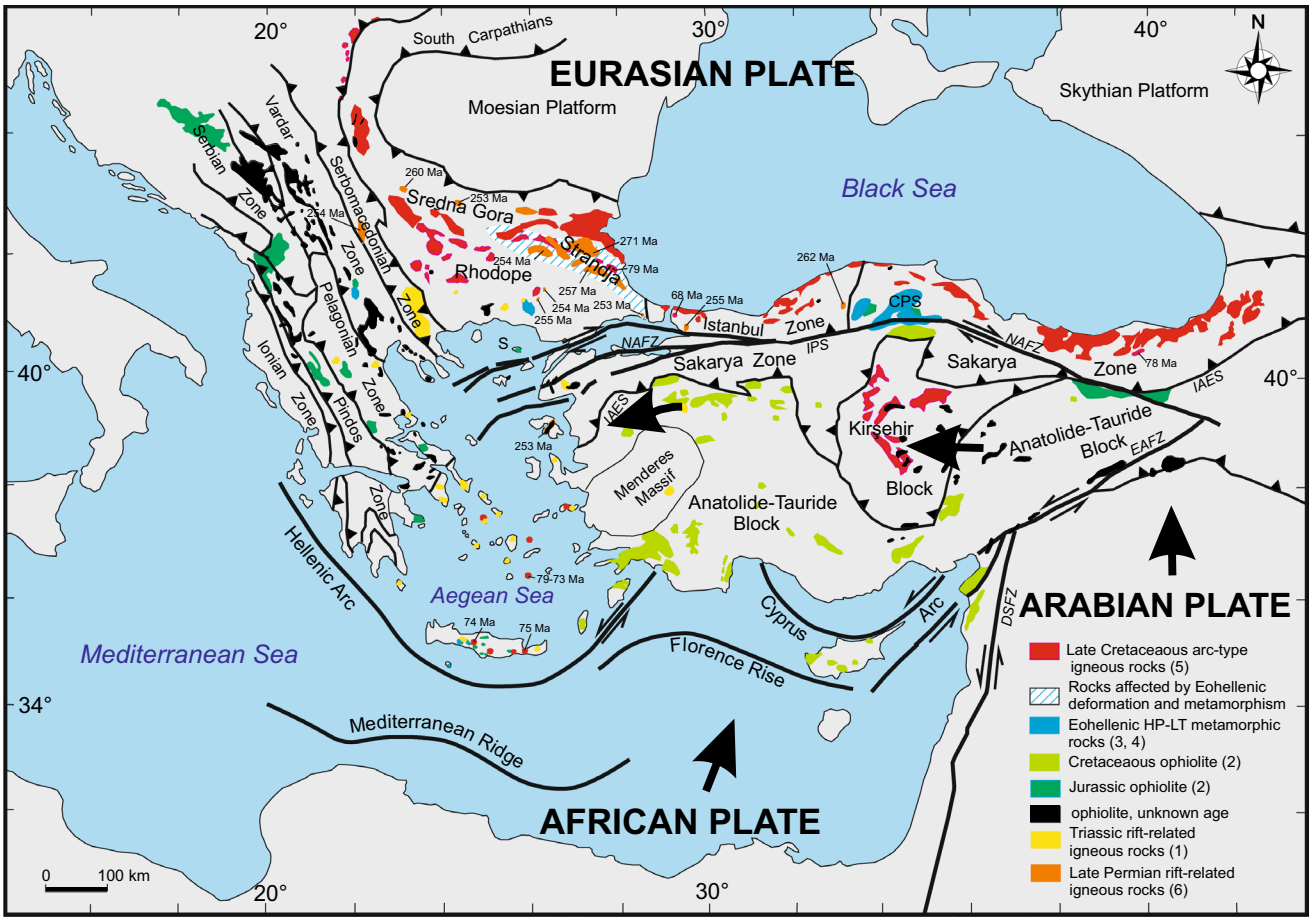

Fig. 10 Distinct rock types of Eastern Mediterranean, which are critical for the provenance of the Uppermost Unit of Crete: (1) Triassic volcanic rocks and granitoids, (Bröcker and Keasling 2006; Bröcker and Pidgeon 2007; Himmerkus et al. 2006; Bulle et al. 2010; Akal et al. 2011; Chatzaras et al. 2012; Liati et al. 2013; Zulauf et al. 2013, 2023a; Bonev et al. 2019; this study); (2) Mesozoic ophiolites (Robertson 2002, and references therein; Liati et al. 2004; Smith 2006, and references therein; Koglin et al. 2009a; Robertson et al. 2012, and references therein); (3) Late Jurassic/early Cretaceous HP–LT metamorphic rocks of the Internal Hellenides (after Seidel et al. 1976, 1977; Michard et al. 1994; Wawrzenitz and Mposkos 1997; Most et al. 2001; Most 2003; Kydonakis et al. 2015; Liati et al. 2016; Altherr et al. 2023); (4) Late Jurassic and Early Cretaceous HP–LT metamorphic rocks of the CPS (Aygül et al. 2016, and references therein); (5) Upper Cretaceous (arc-type) magmatic rocks (von Quadt et al. 2005, 2007, and references therein; Okay and Nikishin 2015, and references therein; Kneuker et al. 2015; Martha et al. 2016, 2017). (6) Permian igneous rocks (Reischmann 1998; Liati 2005; Koglin et al. 2009b, Tanatsiev et al. 2012; Okay and Nikishin 2015, and references therein; Antic et al. 2015, 2016; Bonev et al. 2019; Lazarova et al. 2021; Salacinska et al. 2021). CPS = Central Pontides Supercomplex; DSFZ = Death Sea fault zone; EASZ = East Anatolian fault zone; IPS = Intrapontide suture; IAES = Izmir–Ankara–Erzincan suture; NAFZ = North Anatolian fault zone; S = Samothraki ophiolite

Late Cretaceous arc-type granitoids and provenance of the Asterousia Crystalline Complex

Besides the late Permian detrital zircons, the Late Cretaceous arc-type granitoids and their host rocks are important tracers to unravel the provenance of the Greenschist Unit and of the ACC of Crete. Cretaceous HT–LP metamorphic rocks and Campanian I-type (meta)granitoids are main constituents of the ACC (Seidel et al. 1976, 1981; Langosch et al. 2000; Kneuker et al. 2015; Martha et al. 2017, 2019). The new U–Pb zircon ages of both sill and dike of the ACC near Lentas are almost the same within uncertainties and suggest emplacement between 72.0 and 73.0 Ma. A monzogranitic vein, which cuts through metasediments of the ACC in the Melambes area (Fig. 2d Supplement), yielded a concordia age at 74.1 ± 0.3 Ma (Martha et al. 2017). Compared to the range of U–Pb zircon ages obtained from the large metagranitoid bodies of the ACC (71–77 Ma, Melambes area, Martha et al. 2017; 72–76 Ma, Pefkos area, Martha et al. 2019, 74–75 Ma, northern Ierapetra Graben, Kneuker et al. 2015), the new U–Pb zircon ages of the igneous veins fit with the younger ages of these bodies, which seems to be reasonable because some of the large granitoid bodies are also cut by igneous veins and are ductility deformed, particularly if quartz is present as a constituent phase. Besides the granitoids, which were emplaced at upper structural

levels (e.g., those of the northern Ierapetra Graben, Kneuker et al. 2015), deformation of the large granitoid bodies took place under similarly high temperatures (> 600 °C, Martha et al. 2017, 2019) like those obtained from the igneous veins of the present study. Folding and boudinage of these veins indicate post-emplacement deformation that is younger than the dominant foliation and the pervasive high-temperature deformation of the metasedimentary host rocks. Nevertheless, the deformation microfabrics of the constituent minerals of the veins suggest that folding and boudinage occurred at still high temperature close to the metamorphic peak. Replacement of K-feldspar by myrmekite is evidence for diffusion-assisted deformation (Simpson and Wintsch 1989; Vernon 1991; Ceccato et al. 2018), which occurs at $T >$ 450–500 °C (Cisneros-Lazaro et al. 2019). Partial recrystallization of feldspar suggests $T >$ ca. 500 °C, and chessboard-type subgrains in quartz indicate deformation at $T >$ 600 °C (see references above). Moreover, lobate phase boundaries between quartz and K-feldspar should result from solid-state diffusion creep (e.g., Gower and Simpson 1992; Kruse and Stünitz 1999; Zulauf et al. 2022), which is also consistent with deformation at high temperature. Thus, boudinage of subhorizontal veins (sills) and folding of subvertical veins (dikes) occurred at deeper structural levels under amphibolite facies conditions. Boudinage of subhorizontal competent layers reflects vertical shortening and horizontal extension of the ACC-type rocks. Similar competent sheets, which are affected by boudinage, are subhorizontal quartz veins and calc-silicate layers (Martha et al. 2017). K–Ar ages of amphibole of these ACC rocks are ca. 70 Ma (Seidel et al. 1976). Thus, deformation of the igneous veins should have occurred in Late Cretaceous (Campanian) times between 73 and 70 Ma.

Late Cretaceous arc-type granitoids and Late Cretaceous HT–LP metamorphic host rocks are also exposed further to the north in the Upper Cycladic Unit, and both are commonly correlated with the Pelagonian Zone of continental Greece (Bonneau 1972, 1984; Dürr et al. 1978; Soukis and Papanikolaou 2004; Tortorici et al. 2012; Papanikolaou 2021). A Late Cretaceous low-pressure/high-temperature imprint has been described from Donoussa and Ikaria (Altherr et al. 1994) and from Tinos (Patzak et al. 1994). On Anafi, arc-type granitoid emplacement took place between 69 and 76 Ma (U–Pb on zircon, Reinecke et al. 1982; Martha et al. 2016). Late Cretaceous U–Pb zircon ages have also been determined from metaigneous mélange exposed on Samos and Syros (Tomaschek et al. 2003; Bröcker and Keasling 2006; Bröcker et al. 2014). Late Cretaceous igneous rocks and Late Cretaceous HT–LP metamorphic rocks, however, have not been described from the Pelagonian Zone of continental Greece, which consists of Triassic to Jurassic carbonates resting below late Jurassic to Early Cretaceous (Eo–Hellenic) wildflysch and ophiolite, which are covered by Late Cretaceous transgressive carbonates and a Late Cretaceous to Eocene flysch (Pe-Piper and Piper 2002; Papanikolaou 2021).

It should be emphasized that the Late Cretaceous arc-type rocks of both Crete and the Cyclades are forming or are part of the Uppermost nappes and thus are allochthonous crustal blocks. Their provenance area is still unclear, but should be located further to the north, beyond the Sava–Vardar–Izmir–Ankara Suture, where a continuous Late Cretaceous magmatic arc ranges from the Lesser Caucasus to the Balkans. This domain is almost the same like that where late Permian rift-related igneous rocks are exposed (Fig. 10). The Late Cretaceous arc magmatism in the Black Sea region lasted from 90 to 70 Ma (Okay and Nikishin 2015). The same holds for the Strandja Massif, Srednogorie and Rhodopes, where the U–Pb zircon ages of granitoids range from 92 to 67 Ma (e.g., von Quadt et al. 2005, 2007). Late Cretaceous calc-alkaline magmatic rocks, known as 'banatites', are present in the Banatitic Magmatic and Metallogenetic Belt of Romania, Serbia and Bulgaria (e.g., Grünenfelder et al. 1983; Soroiu et al. 1986; Ciobanu et al. 2002; Vlad and Berza 2003). This belt is ca. 1.500 km long and ranges from the Strandja Massif via Sredna Gora and south Carpathians until the Apuseni Mountains (Fig. 10).

The detrital zircon age spectra of the Greenschist Unit and of the ACC are different to those reported above. As the quartzites of both also include late Permian and Mesozoic zircons, which extend until Jurassic and Cretaceous times, their maximum deposition age is much younger than that of the Preveli and Vatos rocks. When taking into account the youngest detrital zircon of the *Greenschist Unit* (157 ± 4 Ma), its maximum deposition age should be Late Jurassic. Similar to the Vatos quartzite, Cambrian and Silurian detrital zircons are lacking. The Precambrian age spectrum is almost the same like that of the Minoan-type age spectrum described above from the Preveli metaconglomerate. There is clear evidence for late Variscan magmatic activity in the source area, particularly at the Carboniferous/Permian boundary. Such peaks are also present in the metasedimentary rocks of the Tyros Unit (Zulauf et al. 2018). However, in contrast to the latter, the detrital zircon ages of the Greenschist Unit do not cease in the early Permian, but continue via the middle and late Permian until the Late Triassic (Fig. 9). The same holds for the detrital zircon age spectra of the *ACC* samples, which are similar to those described from the Greenschist Unit above (Fig. 9): (1) The youngest detrital zircons are younger than Triassic, (2) the Precambrian detrital zircons are in line with a Minoan-type age spectrum, (3) all ACC samples include early Paleozoic (Cambro-Ordovician) detrital zircons, (4) Devonian and Carboniferous detrital zircons reflect Variscan magmatism in the source areas, and (5) there is an almost continuous record

of detrital zircon ages from Carboniferous to the Triassic or even to the Jurassic or Cretaceous.

The Devonian and Carboniferous detrital zircons of the ACC-type rocks may have come directly from exposed magmatic host rocks or they were recycled from Triassic or Permian metasedimentary rocks of the hinterland. The Triassic detrital zircon ages of the quartzite of the Greenschist Unit and those of the ACC are matching well the U–Pb ages of skarn-grandite and of zircon of felsic metavolcanic rocks of the Preveli Unit (Zulauf et al. 2023a). Moreover, igneous rocks with similar protolith ages have been described from the Cycladic Blueschist Unit (Naxos, Reischmann 1998; Syros, Tomaschek et al. 2001; Andros, Ios and Sifnos, Bröcker and Pidgeon 2007).

To shed light on the source area of the rocks of the Greenschist Unit and of the ACC, we should focus on the presence of late Permian zircons, which are largely lacking in the Tyros Unit of the External Hellenides (Zulauf et al. 2013, 2018), but are present in the Cyclades, where rocks with similar young maximum deposition age are exposed. Detrital zircon U–Pb ages in the Cycladic Blueschist Unit suggest Triassic to Late Cretaceous depositional ages (Löwen et al. 2015; Bröcker et al. 2016; Hinsken et al. 2015; Seman et al. 2017; Flansburg et al. 2019; Poulaki et al. 2019; Laskari et al. 2022). The Cretaceous metasediments of the Cycladic Blueschist Unit include late Permian detrital zircons (Hinsken et al. 2015; Seman et al. 2017; Flansburg et al. 2019; Poulaki et al. 2019; Laskari et al. 2022). The same holds for the Makrotantalon Unit of Andros, where U–Pb dating of detrital zircons yielded ca. 260 Ma (unpublished data cited in Huyskens and Bröcker 2014). In the western Cyclades, flysch-type rocks of the Cycladic Blueschist Unit with Late Jurassic to Cretaceous maximum deposition age and Paleozoic detrital zircons include late Permian detrital zircons (Seman et al. 2017). These flysch-type sediments could be equivalents of the Greenschist Unit and of the ACC rocks of Crete. Late Permian detrital zircons have also been detected in Triassic sedimentary rocks of the Sakarya Zone of NW Turkey (Ustaömer et al. 2016).

However, neither in the Sakarya Zone nor in the Cyclades or in the Pelagonian Zone of mainland Greece, late Permian igneous rocks are exposed. The same holds for Crete. Late Permian (ca. 260 Ma) rift-related granitoids are present further to the north in the Istanbul Zone, Strandja Massif and Dobrogea, most of which extended into Triassic times (Fig. 10; Nikishin et al. 2002; Okay and Nikishin 2015 and references therein; Sałacińska et al. 2021). Late Permian igneous activity is further documented on Lesvos (Koglin et al. 2009b), in the Serbo-Macedonian Zone (Antić et al. 2015, 2016), in the Rhodope (Liati 2005; Bonev et al. 2019), in the Sredna Gora Mountains (Tanatsiev et al. 2012; Lazarova et al. 2021) and in the western Carpathians (Vozárová et al. 2020; Ondrejka et al. 2021; Villaseñor et al. 2021). Finally, similar late Permian U–Pb zircon ages have been derived from A-type rhyolites in the Silicic Unit of Slovakia (Ondrejka et al. 2018), volcanic dikes in the Tatric/Infratatric Units (Putiš et al. 2016; Pelech et al. 2017), rhyodacitic volcanics of the Tisza Mega-Unit, Hungary (Szemerédi et al. 2020) and the Romanian Carpathians (Pană et al. 2002).

As late Permian detrital zircons and Late Cretaceous arc-type granitoids are main constituents of the Greenschist Unit and of the ACC of Crete, their provenance area should be located inside the late Permian/Late Cretaceous igneous belt described above (Fig. 10). The same holds for the Talea Ori group of central Crete. Detrital zircons of the Bali and Sisses Formation of the lower Talea Ori group display middle/late Permian ages (ca. 269 Ma, Zulauf et al. 2016; Seybold et al. 2019), which are compatible with a provenance in NW Turkey as suggested by Seybold et al. (2019). Thus, the Talea Ori group can also be attributed to the Uppermost Unit of Crete.

The role of the North Anatolian Fault Zone

Although the rocks of the Vardar–Serbo–Macedonian–Rhodope domain are similar to those of the Uppermost Unit of Crete, a correlation is questionable because the Late Jurassic/Early Cretaceous blueschists of mainland Greece have been thrust on top of the Pelagonian Zone (Most 2003), which rests on top of Pindos rocks. On Crete, on the other hand, the Uppermost Unit is resting directly on the Pindos nappe, whereas the Pelagonian Zone is lacking. Moreover, the distance between the Vardar–Serbo-Macedonian–Rhodope area and Crete is ca. 700 km, and significant parts of the tectonic nappe transport in northern Greece were accommodated by SW-directed thrusting (Burg 2012, and references therein, Kydonakis et al. 2015) (Fig. 10).

Possible equivalents of the Uppermost Unit of Crete, previously situated in the Pontides or in the southern prolongation of the Strandja Zone, might have been shifted towards Crete during the westward/southwestward counterclockwise movement of the Anatolian block related to dextral strike–slip along the North Anatolian Fault Zone. In NW Turkey the North Anatolian Fault Zone might have initiated as a dominantly N–S-extensional system that later evolved into a strike–slip fault (Le Pichon et al. 2016). Shear-related basins along the Southern Strand are late Miocene in age (Şengör et al. 2005). K–Ar and $^{40}Ar/^{39}Ar$-dating of authigenic illite (Uysal et al. 2006; Boles et al. 2015) as well as structural and isotopic data of the Eskişhehir and Kapıdağ shear zone (Okay et al. 2008; Türkoğlu et al. 2016), however, suggest that the dextral movement along the North Anatolian Fault Zone started already in Eocene times, which is consistent with the formation of Eocene pull-apart basins (Ottria et al. 2017). Due to dextral slip along the North Anatolian

Fault Zone, slices of the Central Pontide Supercomplex or of similar rocks of the Sakarya Zone or of the Strandja Massif might have been scraped off and translated towards the Pindos basin in the west. Parts of these slices underwent subduction in the Aegean domain (Cyclades), where the main HP–LT metamorphism was initiated at the same Eocene time (e.g., Altherr et al. 1979; Bröcker et al. 1993; Lagos et al. 2007) when dextral slip of the North Anatolian Fault Zone started to be active. The Makrotantalon Unit of Andros might represent such a subducted slice. The Makrotantalon Unit includes marble that yielded Permian fossils (Papanikolaou 1978) and shows evidence for early Cretaceous HP–LT metamorphism (ca. 116 Ma, Huet et al. 2014). As Permian marble and Eohellenic HP–LT metamorphism are also documented in the Preveli Unit of Crete (Bonneau and Lys 1978; Seidel et al. 1977) the latter might form an equivalent of the Makrotantalon Unit.

Thrusting of the Preveli and higher nappes on top of the Pindos Unit in Eocene times was related to top-to-the west movements, which persisted until the early Miocene when the Pindos and Uppermost Unit of Crete were thrust on top of the Tripolitza rocks (Klein et al. 2023). Further movement of these nappes was controlled by slab roll-back and top-to-the south thrusting related to the emplacement of the Tripolitza, Pindos and Uppermost Unit on top of the structurally deeper nappes (Tyros, Pre-Alpine Basement, Phyllite–Quartzite s.str, Typali, Plattenkalk). Such a sequence of nappe emplacement would also explain why fragments of the Late Cretaceous arc—now situated in the Rhodope–Strandja domain and north of the North Anatolian Fault Zone—are major constituents of both the Uppermost Unit of Crete (ACC) and the Upper Cycladic Unit (e.g., Ikaria, Donoussa, Anafi). At present, there is no model and no paleogeographic reconstruction available (e.g., Jolivet and Brun 2008: Fig. 10; van Hinsbergen and Schmid 2012: Fig. 11; Menant et al. 2016), which could explain this peculiar situation.

The U–Pb zircon ages of the reddish granite pebble, that is part of the second Pindos flysch, are consistent with the detrital zircon ages described above. The concordia age at 234 ± 2 Ma is interpreted as the emplacement age of the granite. This emplacement age and the younger inherited zircons (245 ± 6, 246 ± 6) are in line with the age of the felsic volcanic rocks of the Preveli Unit (237 ± 2, 242 ± 1 Ma) and with the Triassic detrital zircons separated from the Greenschist Unit and from the ACC-type rocks. The same holds for the late Permian detrital zircons (262 ± 7 and 271 ± 7 Ma). It should be noted that granitoids with such a Ladinian age have yet not been found in the Pelagonian Zone, but are frequent in the Cyclades, Menderes and Serbo-Macedonian–Rhodope–Strandja domains (Fig. 10). Moreover, the Triassic granite boulder is compatible with slices of Triassic pelagic limestone, described from this nappe contact (Robert and Bonneau 1982). Thus, during the deposition of the Paleocene/Eocene Pindos flysch, the early Triassic granitoids of the Preveli nappe were already exhumed, removed and deposited as olistoliths in the flysch basin. Such a sequence of events is compatible with the Eocene fission-track ages of the Uppermost Unit mentioned above.

Conclusions

Based on the new data and results, the following conclusions can be drawn:

- The detrital zircons of all metasedimentary rocks of the Uppermost Unit of Crete are characterized by a Mionan-type age spectrum and by Carboniferous (Variscan) ages.
- The rocks of the Greenschist Unit and ACC are Jurassic/Cretaceous in age and thus unexpectedly young. Their different degree of LP–HT metamorphism can be explained by Cretaceous slab roll-back, which 'shifted' the Late Cretaceous arc towards the accreted trench and fore-arc deposits portrayed by the Vatos rocks.
- The large amount of late Permian detrital zircons together with the presence of Late Cretaceous arc-type granitoids, suggest that the ACC is derived from the late Permian/Late Cretaceous magmatic belt situated north of the Sava–Vardar–Izmir–Ankara Suture in the Strandja–Rhodope domains.
- The distance between the source area of the Uppermost Unit in the Strandja–Rhodope domains and Crete is more than 500 km. The kinematic data suggest that this large distance of nappe movement was accommodated not only by nappe transport, but also by dextral strike–slip along the North Anatolian Fault Zone and related counterclockwise rotation of the Anatolian block.
- There is clear evidence that the Upper Cycladic Unit is an equivalent of the ACC and Greenschist Unit, while the Makrotantalon Unit of Andros might form a Cycladic equivalent of the Preveli nappe. As the rocks of the Upper Cycladic Unit are also allochthonous crustal blocks, they can be regarded as 'footprints', which are tracking the movement of the Cretan nappes.
- The olistolith of reddish granite within the second Pindos flysch is of Ladinian age and should be derived from the Preveli Unit, which was situated and eroded in the upper plate during Eocene nappe emplacement.
- Future studies should focus on possible source rocks and on the age of the detrital zircons of the Vatos flysch and of the metasediments, which are part of the nappe contact between Preveli and Pindos Unit.

Supplementary Information The online version contains supplementary material available at https://doi.org/10.1007/s00531-023-02356-9.

Acknowledgements We are grateful to Janina Schastok (Universität Frankfurt) for her help with the isotopic analyses. Constructive reviews by N. Koglin, an anonymous referee, and the Chief Editor of IJES (U. Riller) are acknowledged. The study was financially supported by German Science Foundation, DFG (Zu 73-34). This is FIERCE contribution 143.

Author contributions WD, SM, PX and GZ contributed to the study conception and design. WD, SM and GZ collected the samples. WD, RA and PX performed the analysis and interpreted the data. GZ wrote the first draft of the manuscript and all the authors commented on previous versions of the manuscript. All the authors read and approved the final manuscript.

Funding Open Access funding enabled and organized by Projekt DEAL. The studies were supported by a grant of Deutsche Forschungsgemeinschaft (DFG Zu 73-34).

Data availability All data and materials of the present paper are fully available.

Code availability Not applicable.

Declarations

Conflict of interest All the authors declare that they have no conflict of interest.

Ethical approval Not applicable.

Consent to participate Not applicable.

Consent for publication Not applicable.

References

Abdelsalam MG, Liégeois JP, Stern RJ (2002) The Saharan Metacraton. J Afr Earth Sc 34:119–136

Akal C, Koralay OE, Candan O, Oberhänsli R, Chen F (2011) Geodynamic significance of the early Triassic Karaburun granitoid (Western Turkey) for the opening history of Neotethys. Turk J Earth Sci 20:255–271

Altherr R, Schliestedt M, Okrusch M, Seidel E, Kreuzer H, Harre W, Lenz H, Wendt I, Wagner GA (1979) Geochronology of high pressure rocks on Sifnos (Cyclades, Greece). Contrib Mineral Petrol 70:245–255

Altherr R, Kreuzer H, Lenz H, Wendt I, Harre W, Dürr S (1994) Further evidence for a Late-Cretaceous low pressure/high-temperature terrane in the Cyclades, Greece Petrology and geochronology of crystalline rocks from the islands of Donoussa and Ikaria. Chem Erde 54:319–328

Altherr R, Topuz G, Marschall H, Zack T, Ludwig T (2004) Evolution of a tourmaline bearing lawsonite eclogite from the Elekdag area (Central Pontides, N Turkey): evidence for infiltration of slab-derived B-rich fluids during exhumation. Contrib Mineral Petrol 148:409–425

Altherr R, Hanel M, Soder CG, Peters D, Bahl C (2023) Petrology and Tectonic Significance of Epidote Blueschist-Facies Rocks from the Northern Margin of the Pelagonian Unit in the Republic of North Macedonia. J Petrol 64:1–31

Antić M, Peytcheva I, von Quadt A et al (2015) Pre-Alpine evolution of a segment of the North-Gondwanan margin: geochronological and geochemical evidence from the central Serbo-Macedonian Massif. Gondwana Res. https://doi.org/10.1016/j.gr.2015.07.020

Antić M, Peytcheva I, von Quadt A, Kounov A, Trivić B, Serafimovski T, Tasev G, Gerdjikov I, Wetzel A (2016) Pre-Alpine evolution of a segment of the North-Gondwanan margin: geochronological and geochemical evidence from the central Serbo-Macedonian Massif. Int J Earth Sci 36:523–544. https://doi.org/10.1016/j.gr.2015.07.020

Aubouin J, Dercourt J (1965) Sur la géologie de L'Egée: regard sur la Crète (Grèce). Bull Soc Géol France 7:787–821

Avigad D, Kolodner K, McWilliams M, Persing H, Weissbrod T (2003) Origin of northern Gondwana Cambrian sandstone revealed by detrital zircon SHRIMP dating. Geology 31:227–230

Avigad D, Gerdes A, Morag N, Bechstaedt T (2012) Coupled U-Pb–Hf of detrital zircons of Cambrian sandstones from Morocco and Sardinia: implications for provenance and Precambrian crustal evolution of north Gondwana. Gondwana Res 21:690–703

Aygül M, Okay AI, Oberhänsli R, Sudo M (2016) Pre-collisional accretionary growth of the southern Laurasian active margin, Central Pontides, Turkey. Tectonophysics 671:218–234

Be'eri-Shlevin Y, Avigad D, Matthews A (2009) Granitoid intrusion and high temperature metamorphism in the Asteroussia Unit, Anafi Island (Greece): petrology and geochronology. Israel J Earth Sci 58:13–27

Boles A, van der Pluijm B, Mulch A, Mutlu H, Uysal IT, Warr LN (2015) Hydrogen and 40Ar/39Ar isotope evidence for multiple and protracted paleofluid flow events within the long-lived North Anatolian Keirogen (Turkey). Geochem Geophys Geosyst 16:1975–1987. https://doi.org/10.1002/2015GC005810

Bonneau M (1972) La nappe métamorphique de l'Asteroussia, lambeau d'affinités pélagoniennes charrié jusque sur la zone de Tripolitza de la Crète moyenne (Grèce). C R Acad Sc Paris Série D 275:2303–2306

Bonneau M (1973) Les différentes «séries ophiolitifères» de la Crète: une mise au point. C R Acad Sc Paris Série D 276:1249–1252

Bonneau M (1984) Correlation of the Hellenide nappes in the southeast Aegean and their tectonic reconstruction. Geol Soc Lond Spec Publ 17:517–527

Bonneau M, Lys M (1978) Sur la présence de Permien fossilifère dans l'unité de Vatos (Crète); sa nature interne et l'ampleur des charriages dans l'arc égéen. C R Acad Sc Paris Série D 287:423–426

Bonneau M, Beauvais L, Middlemiss FA (1974) L'unité de Miamou (Crète – Grèce) et sa macrofaune d'âge Jurassique supérieur (Brachiopodes, Madréporaires). Ann Soc géol du Nord T XCIV, Scéance du 11 Avril, 71–87, Lille

Bonneau M, Angelier J, Epting M (1977) Réunion extraordinaire de la Société Géologique de France en Crète. Bull Sc Géol France, Série 7(19):87–102

Bonev N, Moritz R, Borisova M, Filipov P (2019) Therma–Volvi–Gomati complex of the Serbo-Macedonian Massif, northern

Greece: a Middle Triassic continental margin ophiolite of Neotethyan origin. J Geol Soc 176:931–944. https://doi.org/10.1144/jgs2017-130
Bröcker M, Franz L (1998) Rb–Sr isotope studies on Tinos Island (Cyclades, Greece): additional time constraints for metamorphism, extent of infiltration-controlled overprinting and deformational activity. Geol Mag 135:369–382
Bröcker M, Franz L (2006) Dating metamorphism and tectonic juxtaposition on Andros Island (Cyclades, Greece): results of a Rb-Sr study. Geol Mag 143:609–620
Bröcker M, Keasling A (2006) Ionprobe U-Pb zircon ages from the high-pressure/low-temperature melange of Syros, Greece: age diversity and the importance of pre-Eocene subduction. J Metamorph Geol 24:615–631
Bröcker M, Pidgeon RT (2007) Protolith ages of meta-igneous and metatuffaceous rocks from the Cycladic Blueschist Unit, Greece: results of a reconnaissance U-Pb zircon study. J Geol 115:83–98
Bröcker M, Kreuzer H, Matthews A, Okrusch M (1993) 40Ar-39Ar and oxygen isotope studies of polymetamorphism from Tinos Island, Cycladic blueschist belt, Greece. J Metamorph Geol 11:223–240
Bröcker M, Löwen K, Rodionov N (2014) Unraveling protolith ages of meta-gabbros from Samos and the Attic-Cycladic Crystalline Belt, Greece: results of a U-Pb zircon and Sr–Nd whole rock study. Lithos 198–199:234–248. https://doi.org/10.1016/j.lithos.2014.03.029
Bröcker M, Huyskens M, Berndt J (2016) U-Pb dating of detrital zircons from Andros, Greece: constraints for the time of sediment accumulation in the northern part of the Cycladic blueschist belt. Geol J 51:354–436
Bulle F, Bröcker M, Gärtner C, Keasling A (2010) Geochemistry and geochronology of HP melanges from Tinos and Andros, Cycladic blueschist belt, Greece. Lithos 117:61–81
Burg J-P (2012) Rhodope: from Mesozoic convergence to Cenozoic extension. Review of petro-structural data in the geochronological frame. J Virtual Explor. https://doi.org/10.3809/jvirtex.2011.00270
Burkhard M (1993) Calcite twins, their geometry, appearance and significance as stress-strain markers and indicators of tectonic regime: a review. J Struct Geol 15:351–368
Catzaras V, Dörr W, Gerdes A, Krahl J, Xypolias P, Zulauf G (2016) Tracking the late Paleozoic to early Mesozoic margin of northern Gondwana in the Hellenides: paleotectonic constraints from U-Pb detrital zircon ages. Int J Earth Sci 105:1881–1900. https://doi.org/10.1007/s00531-016-1298-z
Ceccato A, Menegon L, Pennacchioni G, Morales LFG (2018) Myrmekite and strain weakening in granitoid mylonites. Solid Earth 9:1399–1419. https://doi.org/10.5194/se-2018-70
Chatzaras V, Dörr W, Finger F, Xypolias P, Zulauf G (2012) U-Pb single zircon ages and geochemistry of metagranitoid rocks in the Cycladic Blueschists (Evia Island): implications for the Triassic tectonic setting of Greece. Tectonophysics 595(596):125–139. https://doi.org/10.1016/j.tecto.2012.05.016
Ciobanu CL, Cook NJ, Stein H (2002) Regional setting and geochronology of the Late Cretaceous Banatitic Magmatic and Metallogenetic Belt. Miner Deposita 37:541–567
Cisneros-Lazaro DG, Miller JA, Baumgartner LP (2019) Role of myrmekite and associated deformation fabrics in controlling development of granitic mylonites in the Pofadder Shear Zone of southern Namibia. Contrib Mineral Petrol 174:22. https://doi.org/10.1007/s00410-019-1555-9
Davi E, Bonneau M (1972) Geological map of Greece 1:50 000 sheet andiskarion. Institute of Geology and Mineral Exploration, Athens
Dickinson WR, Gehrels GE (2009) Use of U-Pb ages of detrital zircons to infer maximum depositional ages of strata: a test against a Colorado plateau Mesozoic database. Earth Planet Sci Lett 288:115–125
Dörr W, Stein E (2019) Precambrian basement in the Rheic suture zone of the Central European Variscides (Odenwald). Int J Earth Sci 108:1937–1957. https://doi.org/10.1007/s00531-019-01741-7
Dörr W, Zulauf G, Gerdes A, Lahaye Y, Kowalczyk G (2015) A hidden Tonian basement in the eastern Mediterranean: age constraints from U-Pb data of magmatic and detrital zircons of the External Hellenides (Crete and Peloponnesus). Precambr Res 258:83–108. https://doi.org/10.1016/j.precamres.2014.12.015
Dürr S (1985) Γεωλογικός χάρτης της Ελλάδος 1:50000 Φύλλο Αμοργός–Δονούσα [Geological map of Greece 1:50,000 Amorgos–Donoussa sheet] Αθήνα [Athens]: Ινστιτούτο γεωλογικών και μεταλλεύτικων έρευνων [Institute of Geology and Mineral Exploration]
Dürr S, Seidel E, Kreuzer H, Harre W (1978) Témoins d'un métamorphisme d'âge crétacé supérieur dans l'Égéide: datations radiométriques de minéraux provenant de l'île de Nikouriá (Cyclades, Grèce). Bull Sc Géol France, Série 7/20(2):209–213
Flansburg ME, Stockli DF, Poulaki EM, Soukis K (2019) Tectonomagmatic and stratigraphic evolution of the Cycladic Basement, Ios Island, Greece. Tectonics 38:2291–2316
Fritz H, Abdelsalam M, Ali KA, Bingen B, Collins AS, Fowler AR, Ghebreab W, Hauzenberger CA, Johnson PR, Kusky TM, Macey P, Muhongo S, Stern RJ, Viola G (2013) Orogen styles in the East African Orogen: a review of the Neoproterozoic to Cambrian tectonic evolution. J Afr Earth Sc 86:65–106
Gerogiannis N, Xypolias P, Chatzaras V, Aravadinou E, Papapavlou K (2019) Deformation within the Cycladic subduction-exhumation channel: new insights from the enigmatic Makrotantalo nappe (Andros, Aegean). Int J Earth Sci 108:817–843. https://doi.org/10.1007/s00531-019-01680-3
Gower RJW, Simpson C (1992) Phase boundary mobility in naturally deformed, high-grade quartzofeldspathic rocks: evidence for diffusional creep. J Struct Geol 14:301–314
Grünenfelder M, Popescu G, Soroiu M, Arsenescu V, Berza T (1983) K-Ar and U–Pb dating of the metamorphic formations and the associated igneous bodies of the central South Carpathians. Ann Inst Géol Géophys 61:37–46
Heinrichs T, Siegesmund S, Frei D, Drobe M, Schulz B (2012) Provenance signatures from whole-rock geochemistry and detrital zircon ages of metasediments from the Austroalpine basement south of the Tauern Window (Eastern Tyrol, Austria). Geo Alp 9(2012):156–185
Himmerkus F, Reischmann T, Kostopoulos D (2009) Triassic rift related meta-granites in the Internal Hellenides, Greece. Geol Mag 146:252–265. https://doi.org/10.1017/S001675680800592X
Hinsken T, Bröcker M, Berndt J, Gärtner C (2015) Maximum sedimentation ages and provenance of metasedimentary rocks from Tinos Island, Cycladic blueschist belt, Greece. Int J Earth Sci. https://doi.org/10.1007/s00531-015-1258-z
Huet B, Labrousse L, Monjé P, Malvoisin B, Jolivet L (2014) Coupled phengite 40Ar-39Ar geochronology and thermobarometry: PTt evolution of Andros Island (Cyclades, Greece). Geol Mag 152:711–727
Huyskens MH, Bröcker M (2014) The status of the Makrotantalon Unit (Andros, Greece) within the structural framework of the Attic-Cycladic Crystalline Belt. Geol Mag 151:430–446. https://doi.org/10.1017/S0016756813000307
Jackson SE, Pearson NJ, Griffin WL, Belousova E (2004) The application of laser ablation-inductively coupled plasma-mass spectrometry to in situ U-Pb Zircon geochronology. Chem Geol 211:47–69. https://doi.org/10.1016/j.chemgeo.2004.06.017
Johnson PR, Andresen A, Collins AS, Fowler AR, Fritz H, Ghebreab W, Kusky T, Stern RJ (2011) Late Cryogenian-Ediacaran history of the Arabian-Nubian Shield: a review of depositional, plutonic,

structural, and tectonic events in the closing stages of the northern East African Orogen. J Afr Earth Sc 61:167–232
Jolivet L, Brun J-P (2008) Cenozoic geodynamic evolution of the Aegean. Int J Earth Sci. https://doi.org/10.1007/s00531-008-0366-4
Karakitzios V (1988) Sur l'existence d'une serie a affinities internes dans la region de Sellia. Ann Géol Pays Hellén 33(1987/1988):217–222
Keay S, Lister GS (2002) African provenance for the metasediments and metaigneous rocks of the Cyclades, Aegean Sea, Greece. Geology 30:235–238
Klein T, Zulauf G, Evans D, Gerdes A, Glodny J, Heidelbach F, Kirst F, Linckens J, Müller W, Özcan E, Petschick R, Xypolias P (2023) Cenozoic evolution of the Tripolitza carbonate platform in the Tethyan realm: new age constraints on deposition, diagenesis, metamorphism and nappe emplacement based on U-Pb and Rb-Sr dating (External Hellenides, Crete). Geol Mag. https://doi.org/10.1017/S0016756823000377
Kneuker T, Dörr W, Petschick R, Zulauf G (2015) Upper crustal emplacement and deformation of granitoids inside the Uppermost Unit of the Cretan nappe stack: constraints from U-Pb zircon dating, microfabrics and paleostress analyses. Int J Earth Sci 104:351–367
Koepke J (1986) Die Ophiolithe der südägäischen Inselbrücke PhD thesis, Technical University of Braunschweig, Germany, 204 pp
Koepke J, Seidel E, Stöckhert B (1997) Epidote-Blueschists and Metasediments of presumably Jurassic age in the uppermost tectonic unit on Crete (Preveli, Central Crete, Greece). Terra Nova, Abstr Suppl 1(9):384
Koepke J, Seidel E, Kreuzer H (2002) Ophiolites on the southern Aegean islands Crete, Karpathos and Rhodes: composition, geochronology and position within the ophiolite belts of the Eastern Mediterranean. Lithos 65:183–203
Koglin N, Kostopoulos D, Reischmann T (2009a) Geochemistry, petrogenesis and tectonic setting of the Samothraki ophiolite, NE Greece: trace-element, isotopic and zircon age constraints. Tectonophysics 473:53–68
Koglin N, Kostopoulos D, Reischmann T (2009b) The Lesvos mafic–ultramafic complex, Greece: Ophiolite or incipient rift? Lithos 108:243–261
Koralay OE, Satır M, Dora OÖ (2001) Geochemical and geochronological evidence for Early Triassic calc-alkaline magmatism in the Menderes Massif, western Turkey. Int J Earth Sci 89:822–835
Krahl J, Herbart H and Katzenberger S (1982) Subdivision of the allochthonous 'Ophiolites'-bearing formation upon the Pindos Group, southwestern part of Central-Crete, Greece In: International Symposium on the Hellenic Arc and Trench (HEAT) April 8–10 1981, Athens Proceedings Volume 1, p 324–341 Αθήνα [Athens]: Εθνικό Μετσόβιο Πολυτεχνείο [Ethnikó Metsóvio Polytechneío]
Krogh TE (1973) A low-contamination method for hydrothermal dissolution of Zircon and extraction of U and Pb for isotopic age determinations. Geochim Cosmochim Acta 37:485–494. https://doi.org/10.1016/0016-7037(73)90213-5
Kröner A, Stern RJ (2005) Pan-African Orogeny. Encyclopedia of geology, vol 1. Elsevier, Amsterdam, pp 1–12
Kruhl JH (1996) Prsim- and basal-plane parallel subgrain boundaries in quartz: a microstructural geothermobarometer. J Metamorph Geol 14:581–589
Kruse R, Stünitz H (1999) Deformation mechanisms and phase distribution in mafic high-temperature mylonites from the Jotun Nappe, southern Norway. Tectonophysics 303:223–249
Küster D, Liégeois J-P, Matukov D, Sergeev S, Lucassen F (2008) Zircon geochronology and Sr, Nd, Pb isotope geochemistry of granitoids from Bayuda Desert and Sabaloka (Sudan): evidence for a Bayudian event (920–900 Ma) preceding the Pan-African orogenic cycle (860–590 Ma) at the eastern boundary of the Saharan Metacraton. Precambr Res 164:16–39
Kydonakis K, Brun J-P, Sokoutis D, Gueydan F (2015) Kinematics of Cretaceous subduction and exhumation in the western Rhodope (Chalkidiki block). Tectonophysics 665:218–235
Lagos M, Scherer EE, Tomaschek F (2007) High precision Lu-Hf geochronology of Eocene eclogite-facies rocks from Syros, Cyclades, Greece. Chem Geol 243:16–35
Lamont TN, Roberts NMW, Searle MP, Gopon P, Waters DJ, Millar I (2020) The age, origin, and emplacement of the Tsiknias Ophiolite, Tinos, Greece. Tectonics. https://doi.org/10.1029/2019TC005677
Langosch A, Seidel E, Stosch H-G, Okrusch M (2000) Intrusive rocks in the ophiolitic mélange of Crete - Witnesses to a Late Cretaceous thermal event of enigmatic geological position. Contrib Mineral Petrol 139:339–355
Laskari S, Soukis K, Lozios S, Stockli DF, Poulaki EM, Stouraiti C (2022) Structural study and detrital zircon provenance analysis of the Cycladic Blueschist Unit Rocks from Iraklia Island: from the Paleozoic Basement Unroofing to the Cenozoic Exhumation. Minerals 12:83. https://doi.org/10.3390/min12010083
Lazarova A, Broska I, Svojtka M, Naydenov K (2021) Klisura/Rozino granite, Central Sredna Gora: a part of the story of late Permian-Early Triassic extensional magmatic event. Rev Bulg Geol Soc 82(3):87–90
LePichon XL, Şengör AMC, Kende J, İmren C, Henry P, Grall C, Karabulut H (2016) Propagation of a strike slip plate boundary within an extensional environment: the westward propagation of the North Anatolian Fault. Can J Earth Sci. https://doi.org/10.1139/cjes-2015-0129
Liati A (2005) Identification of repeated Alpine (ultra) high-pressure metamorphic events by U-Pb SHRIMP geochronology and REE geochemistry of zircon: the Rhodope zone of Northern Greece. Contrib Miner Petrol 150:608–630
Liati A, Gebauer D, Fanning CM (2004) The age of ophiolitic rocks of the Hellenides (Vourinos, Pindos, Crete): first U-Pb ion microprobe (SHRIMP) zircon ages. Chem Geol 207:171–188
Liati A, Skarpelis N, Fanning MC (2013) Late Permian-Early Triassic igneous activity in the Attic Cycladic Belt (Attica): new geochronological data and geodynamic implications. Tectonophysics 595–596:140–147
Liati A, Theye T, Fanning CM, Gebauer D, Rayner N (2016) Multiple subduction cycles in the Alpine orogeny, as recorded in single zircon crystals (Rhodope zone, Greece). Gondwana Res 29:199–207
Löwen K, Bröcker M, Jasper B (2015) Depositional ages of clastic metasediments from Samos and Syros, Greece: results of a detrital zircon study. Int J Earth Sci 104:205–220. https://doi.org/10.1007/s00531-014-1058-x
Ludwig KR (1994) Isoplot—a plotting and regression program for radiogenic-isotope data. Version 2.75: US Geological Survey Open-File Report 91–445
Ludwig KR (2001) Isoplot/Ex—a geochronological toolkit for Microsoft Excel. Berkley Geochronology Center Special Publication
Mainprice D, Bouchez J-L, Blumenfeld P, Tubia J (1986) Dominant c-slip in naturally deformed quartz: implications for dramatic plastic softening at high temperatures. Geology 14:819–822
Malten HS (2019) Strukturgeologische und petrologische Untersuchungen der Spili- und Vatos-Schichten innerhalb der Uppermost Unit im Raum Vatos Ardaktos, Zentralkreta (Griechenland). Master thesis, Goethe University Frankfurt a.M., Germany, 45 pp (unpublished)
Martha SO, Dörr W, Gerdes A, Petschick R, Schastock J, Xypolias P, Zulauf G (2016) New structural and U-Pb zircon data from Anafi crystalline basement (Cyclades, Greece): constraints on

the evolution of a Late Cretaceous magmatic arc in the Internal Hellenides. Int J Earth Sci 105:2031–2060. https://doi.org/10.1007/s00531-016-1346-8

Martha SO, Dörr W, Gerdes A, Krahl J, Linckens J, Zulauf G (2017) The tectonometamorphic and magmatic evolution of the Uppermost Unit in central Crete (Melambes area): constraints on a Late Cretaceous magmatic arc in the Internal Hellenides (Greece). Gondwana Res 48:50–71. https://doi.org/10.1016/j.gr.2017.04.004

Martha SO, Zulauf G, Dörr W, Binck JJ, Nowara PM, Xypolias P (2019) The tectonometamorphic evolution of the Uppermost Unit south of the Dikti Mountains, Crete. Geol Mag 156:1003–1026. https://doi.org/10.1017/S0016756818000328

Marsellos AE, Foster DA, Kamenov GD, Kyriakopoulos K (2012) Detrital zircon U–Pb data from the Hellenic south Aegean belts: constraints on the age and source of the South Aegean basement. J Virt Expl 42. https://doi.org/10.3809/jvirtex.2011.00284 (paper 3)

Meinhold G, Kostopoulos D, Frei D, Himmerkus F, Reischmann T (2010) U-Pb LASF-ICP-MS zircon geochronology of the Serbo-Macedonian Massif, Greece: palaeotectonic constraints for Gondwana-derived terranes in the Eastern Mediterranean. Int J Earth Sci 99:813–832

Meinhold G, Morton AC, Avigad D (2013) New insights into peri-Gondwana paleogeography and the Gondwana super-fan system from detrital zircon U-Pb ages. Gondwana Res 23:661–665

Meinhold G, Bassis A, Hinderer M, Lewin A, Berndt J (2021) Detrital zircon provenance of north Gondwana Palaeozoic sandstones from Saudi Arabia. Geol Mag 158:442–458. https://doi.org/10.1017/S0016756820000576

Menant A, Jolivet L, Vrielynck B (2016) Kinematic reconstructions and magmatic evolution illuminating crustal and mantle dynamics of the eastern Mediterranean region since the late Cretaceous. Tectonophysics 675:103–140

Michard A, Goffe B, Liati A, Mountrakis D (1994) Blueschist-facies assemblages in the peri-Rhodopian zone and hints for an Eohellenic HP/LT belt in Northern Greece. Bull Geol Soc Greece 30(1):185–192

Most T (2003) Geodynamic evolution of the Eastern Pelagonian zone in Northwestern Greece and the republic of Macedonia. PhD thesis, Tübingen University, Germany

Most T, Frisch W, Dunkl I, Kodosa B, Boev B, Avgerinas A, Kilias A (2001) Geochonological and structural investigation of the Northern Pelagonian crystalline zone Constraints from K/Ar and zircon and apatite fission track dating. Bull Geol Soc Greece 34:91–95

Mposkos E, Krohe A, Baziotis I (2021) Deep tectonics in the Eastern Hellenides uncovered: The record of Variscan continental amalgamation, Permo-Triassic rifting, and Early Alpine collision in Pre-Variscan continental crust in the W-Rhodope (Vertiscos-Ograzden Complex N, Greece). Tectonics. https://doi.org/10.1029/2019TC005557

Nasdala L, Hofmeister W, Norberg N, Mattinson JM, Corfu F, Dörr W et al (2008) Zircon M257 - a Homogeneous natural reference material for the Ion Microprobe U-Pb analysis of zircon. Geostand Geoanal Res 32:247–265

Neuwirth N (2018) Structural Investigation of the Asteroussia Crystalline Complex near Lendas. Master Thesis, Goethe University Frankfurt a.M., Germany; 39 pp

Nikishin AM, Ziegler PA, Abbott D, Brunet M-F, Cloetingh S (2002) Permo-Triassic intraplate magmatism and rifting in Eurasia: implications for mantle plumes and mantle dynamics. Tectonophysics 351:3–39. https://doi.org/10.1016/S0040-1951(02)00123-3

Okay AI, Nikishin AM (2015) Tectonic evolution of the southern margin of Laurasia in the Black Sea region. Int Geol Rev. https://doi.org/10.1080/00206814.2015.1010609

Okay AI, Satır M, Tüysüz O, Akyüz S, Chen F (2001) The tectonics of the Strandja Massif: late-Variscan and mid-Mesozoic deformation and metamorphism in the northern Aegean. Int J Earth Sci 90:217–233. https://doi.org/10.1007/s005310000104

Okay AI, Tüysüz O, Satır M, Özkan-Altıner S, Altıner D, Sherlock S, Eren RH (2006) Cretaceous and Triassic subduction-accretion, HP/LT metamorphism and continental growth in the Central Pontides, Turkey. GSA Bull 118:1247–1269

Okay AI, Satır M, Zattin M, Cavazza W, Topuz G (2008) An Oligocene ductile strike-slip shear zone: the Uludağ Massif, northwest Turkey – Implications for the westward translation of Anatolia. GSA Bull 120:893–911

Okay AI, Sunal G, Sherlock S, Altıner D, Tüysüz O, Kylander-Clark ARC, Aygül M (2013) Early Cretaceous sedimentation and orogeny on the southern active margin of Eurasia: Central Pontides, Turkey. Tectonics 32:1247–1271

Ondrejka M, Li X-H, Vojtko R, Putiš M, Uher P, Sobocký T (2018) Permian A-type rhyolites of the Muráň Nappe, Inner Western Carpathians, Slovakia: in-situ zircon U-Pb SIMS ages and tectonic setting. Geol Carpath 69:187–198. https://doi.org/10.1515/geoca-2018-0011

Ondrejka M, Uher P, Putiš M, Kohút M, Broska I, Larionov A, Bojar A-V, Sobocký T (2021) Permian A-type granites of the Western Carpathians and Transdanubian regions: products of the Pangea supercontinent breakup. Int J Earth Sci 110:2133–2155. https://doi.org/10.1007/s00531-021-02064-2

Ottria G, Pandolfi L, Catanzariti R, Da Prato S, Ellero A, Frassi C, Göncüoğlu MC, Marroni M, Ruffini L, Sayit K (2017) Evolution of an early Eocene pull-apart basin in the Central Pontides (Northern Turkey): New insights into the origin of the North Anatolian Shear Zone. Terra Nova 29:392–400

Palamakumbura RN, Robertson AHF, Dixon JE (2013) Geochemical, sedimentary and micropaleontological evidence for a Late Maastrichtian oceanic seamount within the Pindos ocean (Arvi Unit, S Crete, Greece). Tectonophysics 595–596:250–262. https://doi.org/10.1016/j.tecto.2012.04.019

Pană DI, Heaman LM, Creaser RA, Erdmer P (2002) Pre-Alpine crust in the Apuseni Mountains, Romania: insights from Sm-Nd and U-Pb data. J Geol 110:341–354

Papanikolaou DJ (1978) Contribution to the geology of the Aegean Sea: the island of Andros. Ann Géol Pays Hellén 29:477–553

Papanikolaou DJ (1989) Occurrence of Arvi, Western Thessaly and Orliakas type formations in Argolis. Bull Geol Soc Greece 24:71–84

Papanikolaou DJ (2021) The geology of Greece. Springer, Berlin/Heidelberg, p 2021

Patzak M, Okrusch M, Kreuzer H (1994) The Akrotiri unit on the island of Tinos, Cyclades, Greece: witness to a lost terrane of Late Cretaceous age. N Jb Geol Paläont Abh 194:211–252

Pelech O, Vozárová A, Uher P, Petrík I, Plašienka D, Šarinová K, Rodionov N (2017) Late Permian volcanic dykes in the crystalline basement of the Považský Inovec Mts. (Western Carpathians): U-Th–Pb SHRIMP and monazite chemical dating. Geol Carpath 68(6):530–542. https://doi.org/10.1515/geoca-2017-0035

Pe-Piper G, Piper DJW (2002) The igneous rocks of Greece: The anatomy of an orogen. Beiträge zur regionalen Geologie der Erde, XV, 573 p

Poulaki EM, Stockli DF, Flansburg ME, Soukis K (2019) Zircon U-Pb chronostratigraphy and provenance of the Cycladic Blueschist Unit and Cycladic Basement on Sikinos and Ios Islands, Greece. Tectonics 38:3586–3613

Pozsgai E, Józsa S, Dunkl I, Sebe K, Thamó-Bozsó E, Sajó I, Dezső J, von Eynatten H (2016) Provenance of the Upper Triassic siliciclastics of the Mecsek Mountains and Villány Hills (Pannonian Basin, Hungary): constraints to the Early Mesozoic paleogeography of the Tisza Megaunit. Int J Earth Sci. https://doi.org/10.1007/s00531-016-1406-0

Putiš M, Li J, Ružička P, Ling X, Nemec O (2016) U/Pb SIMS zircon dating of a rhyolite intercalation in Permian siliciclastics as well as a rhyodacite dyke in micaschists (Infratatricum, W. Carpathians). Miner Slov 48:135–144

Reinecke T, Altherr R, Hartung B, Hatzipanagiotou K, Kreuzer H, Harre W, Klein H, Keller J, Geenen E, Böger H (1982) Remnants of a Late Cretaceous high temperature belt on the island of Anafi (Cyclades, Greece). N Jb Mineral Abh 145(2):157–182

Reischmann T (1998) Pre-Alpine origin of tectonic units from the metamorphic complex of Naxos, Greece, identified by single zircon Pb/Pb dating. Bull Geol Soc Greece 32(3):101–111

Robert U, Bonneau M (1982) Les basalts des nappes du Pinde et d' Arvi et leur signification dans l'évolution géodynamique de la Mediterranée orientale. Ann Géol Pays Héllen 31:373–408

Robertson AHF (2002) Overview of the genesis and emplacement of Mesozoic ophiolites in the Eastern Mediterranean Tethyan region. Lithos 65:1–67

Robertson AHF (2012) Late Palaeozoic-Cenozoic tectonic development of Greece and Albania in the context of alternative reconstructions of Tethys in the Eastern Mediterranean region. Int Geol Rev 54(4):373–454. https://doi.org/10.1080/00206814.2010.543791

Romano SS, Dörr W, Zulauf G (2004) Cambrian granitoids in pre-Alpine basement of Crete (Greece): evidence from U-Pb dating of zircon. Int J Earth Sci 93:844–859

Sałacińska A, Gerdjikov I, Gumsley A, Szopa K, Chew D, Gawęda A, Kocjan I (2021) Two stages of Late Carboniferous to Triassic magmatism in the Strandja Zone of Bulgaria and Turkey. Geol Mag 158:2151–2164. https://doi.org/10.1017/S0016756821000650

Seidel E, Okrusch M, Kreuzer H, Raschka H, Harre W (1976) Eo-Alpine metamorphism in the Uppermost Unit of the Cretan nappe system—petrology and geochronology Part 1, The Léndas area (Asteroúsia Mountains). Contrib Mineral Petrol 57:259–275

Seidel E, Schliestedt M, Kreuzer H, Harre W (1977) Metamorphic rocks of late Jurassic age as components of the ophiolitic mélange on Gavdos and Crete (Greece). Geol Jb 28:3–21

Seidel E, Okrusch M, Kreuzer H, Raschka H, Harre W (1981) Eo-Alpine metamorphism in the Uppermost Unit of the Cretan nappe system—petrology and geochronology Part 2 Synopsis of high-temperature metamorphics and associated ophiolites. Contrib Mineral Petrol 76:351–361

Seman S, Stockli DF, Soukis K (2017) The provenance and internal structure of the Cycladic Blueschist Unit revealed by detrital zircon geochronology, Western Cyclades, Greece. Tectonics 36:1407–1429

Şengör AMC, Tüysüz O, İmren C, Sakınç M, Eyidoğan H, Görür N, Le Pichon X, Rangin C (2005) The North Anatolian fault: a new look. Annu Rev Earth Planet Sci 33:37–112. https://doi.org/10.1146/annurevearth32101802120415

Smith AG (2006) Tethyan ophiolite emplacement, Africa to Europe motions, and Atlantic spreading. In: Robertson AHF, Mountrakis D (eds) Tectonic development of the eastern Mediterranean region, vol 260. Geological Society, London, pp 11–35

Seybold L, Dörr W, Trepmann CA, Krahl J (2019) New constraints from U-Pb dating of detrital zircons on the palaeogeographic origin of metasediments in the Talea Ori, central Crete. Geol Mag. https://doi.org/10.1017/S0016756819001365

Simpson C, Wintsch J (1989) Evidence for deformation-induced feldspar by myrmekite. J Metamorph Geol 7:261–275

Soroiu M, Catilina R, Strutinski C (1986) K-Ar ages on some igneous rocks from the south-western end of the South Carpathians (Banat Hills). Rev Roum Phys 31:849–854

Soukis K, Papanikolaou D (2004) Contrasting geometry between Alpine and late- to post-Alpine tectonic structures in Anafi Island (Cyclades). Bull Geol Soc Greece 36:1688–1696

Stacey JS, Kramers JD (1975) Approximation of terrestrial lead isotope evolution by a two-stage model. Earth Planet Sci Lett 26:207–221

Stampfli GM, Hochard C, Vérard C, Wilhelm C, von Raumer J (2013) The formation of Pangea. Tectonophysics 593:1–19

Stern RJ, Ali KA, Liégeois J-P, Johnson P, Wiescek F, Kattan F (2010) Distribution and significance of pre-Neoproterozoic zircons in juvenile Neoproterozoic igneous rocks of the Arabian-Nubian Shield. Am J Sci 310:791–811

Sunal G, Satır M, Natal'in B, Topuz G, Von Der Schmidt O (2011) Metamorphism and diachronous cooling in a contractional orogen: the Strandja Massif, NW Turkey. Geol Mag 148:580–596. https://doi.org/10.1017/S0016756810001020

Szemerédi M, Lukács R, Varga A, Dunkl I, Józsa S, Tatu M, Pál-Molnár E, Szepesi J, Guillong M, Szakmány G, Harangi S (2020) Permian felsic volcanic rocks in the Pannonian Basin (Hungary): new petrographic, geochemical, and geochronological results. Int J Earth Sci 109:101–125. https://doi.org/10.1007/s00531-019-01791-x

Tanatsiev S, Ichev M, Pristavova S (2012) U-Pb zircon dating of the acid volcanic rocks from the Sofia Stara Planina (Balkan) Mountains, West Bulgaria. Bulgarian Geological Society, National Conference "Geosciences 2012", p. 69–70

Thomson SN, Stöckhert B, Rauche H, Brix MR (1998) Apatite fission-track thermochronology of the uppermost tectonic unit of Crete, Greece: implications for the post-Eocene tectonic evolution of the Hellenic subduction system. In: Van Den Haute V, De Corte F (eds) Advances in fission-track geochronology. Kluwer Academic, Dordrecht, pp 187–205

Thomson SN, Stöckhert B, Brix MR (1999) Miocene high-pressure metamorphic rocks of Crete, Greece: rapid exhumation by buoyant escape. Geol Soc Lond Spec Publ 154:87–107

Thorbecke G (1987) Die Zonengliederung der ägäischen Helleniden und westlichen Tauriden Wien: Gesellschaft der Geologie- und Bergbaustudenten in Österreich, 161 pp

Tomaschek F, Kennedy AK, Keay S, Ballhaus C (2001) Geochronological constraints on Carboniferous and Triassic magmatism in the Cyclades: SHRIMP U-Pb ages of zircons from Syros, Greece. J Conf Abstr 6:315

Tomaschek F, Kennedy AK, Villa IM, Lagos M, Ballhaus C (2003) Zircons from Syros, Cyclades, Greece—recrystallization and mobilization of zircon during high-pressure metamorphism. J Petrol 44:1977–2002. https://doi.org/10.1093/petrology/egg067

Tortorici L, Catalano S, Cirrincione R, Tortorici G (2012) The Cretan ophiolite-bearing mélange (Greece): a remnant of Alpine accretionary wedge. Tectonophysics 568–569:320–334

Türkoğlu E, Zulauf G, Linckens J, Ustaömer T (2016) Dextral strike-slip along the Kapıdağ shear zone (NW Turkey): evidence for Eocene westward translation of the Anatolian plate. Int J Earth Sci 105:2061–2074. https://doi.org/10.1007/s00531-016-1372-6

Ustaömer PA, Ustaömer T, Gerdes A, Zulauf G (2011) Detrital zircon ages from a Lower Ordovician quartzite of the Istanbul exotic terrane (NW Turkey): evidence for Amazonian affinity. Int J Earth Sci 100:23–41. https://doi.org/10.1007/s00531-009-0498-1

Ustaömer PA, Ustaömer T, Robertson AHF (2012a) Ion Probe U-Pb Dating of the Central Sakarya Basement: a peri-Gondwana

Terrane intruded by Late Lower Carboniferous Subduction/Collision-related Granitic Rocks. Turkish J Earth Sci 21:905–932

Ustaömer T, Robertson AHF, Ustaömer PA, Gerdes A, Peytecheeva I (2012b) Constraints on Variscan and Cimmerian magmatism and metamorphism in the Pontides (Yusufeli–Artvin area), NE Turkey from U-Pb dating and granite geochemistry. In: Robertson AHF, Parlak O, Ünlügenç UC (eds) Geological development of Anatolia and the Easternmost Mediterranean Region, vol 372. Geological Society London Special Publications, pp 49–74

Ustaömer T, Ustaömer PA, Robertson AHF, Gerdes A (2016) Implications of U-Pb and Lu–Hf isotopic analysis of detrital zircons for the depositional age, provenance and tectonic setting of the Permian-Triassic Palaeotethyan Karakaya Complex, NW Turkey. Int J Earth Sci 105:7–38. https://doi.org/10.1007/s00531-015-1225-8

Uysal IT, Mutlu H, Altunel E, Karabacak V, Golding SD (2006) Clay mineralogical and isotopic (K-Ar, δ18O, δD) constraints on the evolution of the North Anatolian fault zone, Turkey. Earth Planet Sci Lett 243:181–194. https://doi.org/10.1016/j.epsl.2005.12.025

van Hinsbergen DJJ, Schmid SM (2012) Map view restoration of Aegean-West Anatolian accretion and extension since the Eocene. Tectonics. https://doi.org/10.1029/2012TC003132

Vernon RH (1991) Questions about myrmekite in deformed rocks. J Struct Geol 13:979–985

Vicente JC (1970) Étude géologique de l'île de Gavdos (Grèce), la plus méridionale de L'Europe. Bull Soc Géol France 7(12):481–495

Villaseñor G, Catlos EJ, Broska I, Kohút M, Hraško L, Aguiler K, Etzel TM, Kyle R, Stockli DF (2021) Evidence for widespread mid-Permian magmatic activity related to rifting following the Variscan orogeny (Western Carpathians). Lithos. https://doi.org/10.1016/j.lithos.2021.106083

Vlad S-N, Berza T (2003) Banatitic Magmatic and Metallogenetic Belt: Metallogeny of the Romanian Carpathians Segment. Studia Univ Babes-Bolyai Geol XLVIII 1(2003):113–122

von Quadt A, Moritz R, Peytcheva I, Heinrich CA (2005) Geochronology and geodynamics of Late Cretaceous magmatism and Cu–Au mineralization in the Panagyurishte region of the Apuseni–Banat–Timok–Srednogorie belt, Bulgaria. Ore Geol Rev 27:95–126. https://doi.org/10.1016/j.oregeorev.2005.07.024

von Quadt A, Peytcheva I, Heinrich CA, Cvetkovic V, Banjesevic M (2007) Upper Cretaceous magmatic evolution and related Cu-Au mineralization in Bulgaria and Serbia Proceedings of the Ninth Biennial SGA Meeting, Dublin 2007, p 861–864

Vozárová A, Šarinová K, Rodionov N, Vozár J (2020) Zircon U-Pb geochronology from Permian rocks of the Tribeč Mts. (Western Carpathians, Slovakia). Geol Carpath 71:274–287. https://doi.org/10.31577/GeolCarp.71.3.6

Wawrzenitz N, Mposkos E (1997) First evidence for Lower Cretaceous HP/HT-metamorphism in the eastern Rhodope, North Aegean region, North-east Greece. Eur J Mineral 9:659–664

Williams IS, Fiannacca P, Cirrincione R, Pezzino A (2012) Peri-Gondwana origin and early geodynamic history of NE Sicily: a zircon tale from the basement of the Peloritani Mountains. Gondwana Res 22:855–865

Zlatkin O, Avigad D, Gerdes A (2012) Evolution and provenance of Neoproterozoic basement and Lower Paleozoic siliciclastic cover of the Menderes Massif (western Taurides): coupled U-Pb–Hf zircon isotope geochemistry. Gondwana Res. https://doi.org/10.1016/j.gr.2012.05.006

Zlatkin O, Avigad D, Gerdes A (2014) Peri-Amazonian provenance of the Proto-Pelagonian basement (Greece), from zircon U-Pb geochronology and Lu–Hf isotopic geochemistry. Lithos 184–187:379–392

Zulauf G, Dörr W, Fiala J, Romano SS (2007) Crete and the Minoan terranes: age constraints from U-Pb dating of detrital zircons. Geol Soc Am Spec Pap 423:401–409

Zulauf G, Blau J, Dörr W, Klein T, Krahl J, Kustatscher E, Petschik R, van de Schootbrugge B (2013) New U-Pb zircon and biostratigraphic data of the Tyros Unit, eastern Crete: constraints on Triassic palaeogeography and depositional environment of the eastern Mediterranean. Z Dt Ges Geowiss 164(2):337–352

Zulauf G, Dörr W, Fisher-Spurlock SC, Gerdes A, Chatzaras V, Xypolias P (2015) Closure of the Paleotethys in the external Hellenides: constraints from U-Pb ages of magmatic and detrital zircons (Crete). Gondwana Res. https://doi.org/10.1016/j.gr.2014.06.011

Zulauf G, Dörr W, Krahl J, Lahaye Y, Chatzaras V, Xypolias P (2016) U-Pb zircon and biostratigraphic data of high-pressure/low-temperature metamorphic rocks of the Talea Ori: tracking the Paleotethys suture in central Crete, Greece. Int J Earth Sci 105:1901–1922. https://doi.org/10.1007/s00531-016-1307-2

Zulauf G, Dörr W, Marko L, Krahl J (2018) The late Eo-Cimmerian evolution of the External Hellenides: constraints from microfabrics and U-Pb detrital zircon ages of Upper Triassic (meta)sediments (Crete, Greece). Int J Earth Sci. https://doi.org/10.1007/s00531-018-1632-8

Zulauf G, Dörr W, Xypolias P, Gerdes A, Kowalczyk G, Linckens J (2019) Triassic evolution of the western Neotethys: constraints from microfabrics and U-Pb detrital zircon ages of the Plattenkalk Unit (External Hellenides, Greece). Int J Earth Sci 108:2493–2529. https://doi.org/10.1007/s00531-019-01773-z

Zulauf G, Zulauf J, Linckens J, Gerdes A, Hattingen E, Loeckle F, Marschall HR, Steckenreiter L (2022) Development of a synorogenic composite sill at deep structural levels of a magmatic arc (Odenwald, Germany). Part 2: rheological inversion and mullion formation under bulk constriction. J Struct Geol. https://doi.org/10.1016/j.jsg.2022.104525

Zulauf G, Linckens J, Beranoaguirre A, Gerdes A, Krahl J, Marschall HR, Millonig L-L, Neuwirth N, Petschick R, Xypolias P (2023a) Long-term formation of barren skarn in a Triassic extensional setting: Implications for the provenance of the Uppermost Unit of Crete, Greece. Int J Earth Sci. https://doi.org/10.1007/s00531-023-02296-4

Zulauf G, Duretz T, Hezel DC, Krahl J, Linckens J, Marschall HR, Xypolias P (2023b) Low temperature creep of garnet: insights from blueschist-facies skarn of the Preveli nappe (Crete, Greece). J Struct Geol **(in press)**